Current Biology 22, 1–11, January 10, 2012 ©2012 Elsevier Ltd All rights reserved DOI 10.1016/j.cub.2011.12.009

Article

Semaphorin and Eph Receptor Signaling Guide a Series of Cell Movements for Ventral Enclosure in *C. elegans*

Richard Ikegami,[1,4] Kristin Simokat,[2,6] Hong Zheng,[1] Louise Brown,[1] Gian Garriga,[4] Jeff Hardin,[2,3] and Joseph Culotti[1,5,*]

[1]Samuel Lunenfeld Research Institute, Mount Sinai Hospital, 600 University Avenue, Toronto, Ontario M5S 1A8, Canada
[2]Program in Cellular and Molecular Biology
[3]Department of Zoology
University of Wisconsin, 1117 West Johnson Street, Madison WI 53706, USA
[4]Department of Molecular and Cell Biology, University of California, Berkeley, 141 Koshland Hall, Berkeley, CA 94720-3204, USA
[5]Department of Molecular Biology, University of Toronto, Toronto, Ontario M5S 1A8, Canada

Summary

Background: In the last stage of the *Caenorhabditis elegans* body wall closure, an open pocket in the epidermis is closed by the migration of marginal epidermal P/pocket cells to the ventral midline. The cellular and molecular mechanisms of this closure remain unknown.

Results: Cells within the pocket align to form a bridge for migration of contralateral P cell pair P9/10 L,R (and neighboring P cells) to the midline. Bridge formation involves rearrangement of five sister pairs of PLX-2/plexin and VAB-1/Eph receptor expressing "plexin band" cells, of which three pairs form a scaffold for bridge assembly and two pairs form the bridge. Bridge formation requires VAB-1 kinase-dependent extension of presumptive bridge cells over scaffold cells toward the ventral midline. An unassembled *vab-1* null mutant bridge obstructs P cell migration, which is largely overcome by plexin band expression of VAB-1 or VAB-1(delC) (a kinase deletion of VAB-1). VAB-1 also functions redundantly with MAB-20/semaphorin to prevent perdurant gaps between sister plexin band cells that block P cell migration.

Conclusions: The Eph receptor mediates cellular extensions required for bridge formation, independently facilitates P cell migration to the midline, and functions redundantly with PLX-2/plexin to prevent gaps in the bridge used for P9/10 cell migration in body wall closure.

Introduction

Body wall closure defects are a leading cause of human birth defects, yet little is known about the cellular and molecular mechanisms involved [1]. The most studied example of body wall closure is dorsal closure in the *Drosophila* embryo. Dorsal closure occurs by spreading of epidermis from the ventral side to the dorsal midline to enclose the embryo and is largely mediated by DPP/TGF-beta signaling between epidermal cells lining the margins of the advancing epidermis and the underlying amnioserosa [2].

Although there is evidence for the involvement of BMP/TGF-beta signaling in mammalian body wall closure and wound healing [3], it is clear that additional signaling mechanisms, including ephrin signaling [4, 5], are involved in these processes. In spite of the known involvement of specific signaling molecules in mammalian body wall closure, the precise cellular and molecular mechanisms mediated by these molecules are largely unknown.

The *C. elegans* embryo provides a genetically tractable alternative model to analyze body wall closure and resembles *Drosophila* dorsal closure in several respects [3]. Epidermal enclosure in *C. elegans* involves extension, stretching, and migration of a large patch of dorsal epidermoblasts around both sides of the embryo to converge and form a seal at the ventral midline. In the final stage of this process, a ventral opening or pocket in the epidermis, lined with marginal epidermoblasts called P/pocket cells, is closed at the ventral midline (Figures 1 and 2A; see also Figure S1 available online). We are studying the underlying cellular and molecular mechanisms that elicit and guide the migration of the P cells to the ventral midline during pocket closure and that regulate the midline alignment of contralateral P cell partners.

Although conventional TGF-beta signaling is not obviously required for pocket closure in *C. elegans*, the axon guidance and cell association signaling pathways involving semaphorin-2a/MAB-20 [6], its PLX-2/plexin receptor [7], the Eph receptor VAB-1, and the ephrins (EFN-1 to EFN-4) are required for several aspects of this process [6, 8–11]. Previously, George et al. [8] suggested that the ephrin receptor VAB-1 expressed in neuroblasts within the open ventral pocket could facilitate ventral enclosure [8]. These results and the involvement of ephrin signaling in mammalian body wall closure prompted us to examine the cellular and molecular functions that are mediated by these signaling proteins in *C. elegans* pocket closure.

To further our understanding of the role of Eph and semaphorin signaling during ventral enclosure, we examined the expression patterns of VAB-1, the only known Eph receptor in *C. elegans* [8], and PLX-2, one of two known Sema-2a/MAB-20 receptors [7, 12]. We discovered a complex pattern of cell births, divisions, and adhesions mediating wild-type pocket closure and identified the cell-specific functions of VAB-1 and MAB-20 signaling in both pocket closure and P cell alignment. We also uncovered the cause of the synthetic pocket closure defects in double-mutant embryos of semaphorin and Eph receptor signaling. These results clarify the roles that phylogenetically conserved guidance cue receptors play during epidermal enclosure and define, at the level of individual cell types and molecular interactions between them, how epithelial cell migrations are controlled in a living embryo.

Results

Expression Pattern of *vab-1* and *plx-2* and Formation of the Wild-Type Pocket Bridge

Because *vab-1* and *mab-20/semaphorin-2A* mutations affect aspects of pocket closure (see below), we decided to characterize the expression patterns of *vab-1* and *plx-2* during pocket

[6]Present address: Department of Biological Sciences, University of Idaho, PO Box 443051, Moscow, ID 83844, USA
*Correspondence: culotti@lunenfeld.ca

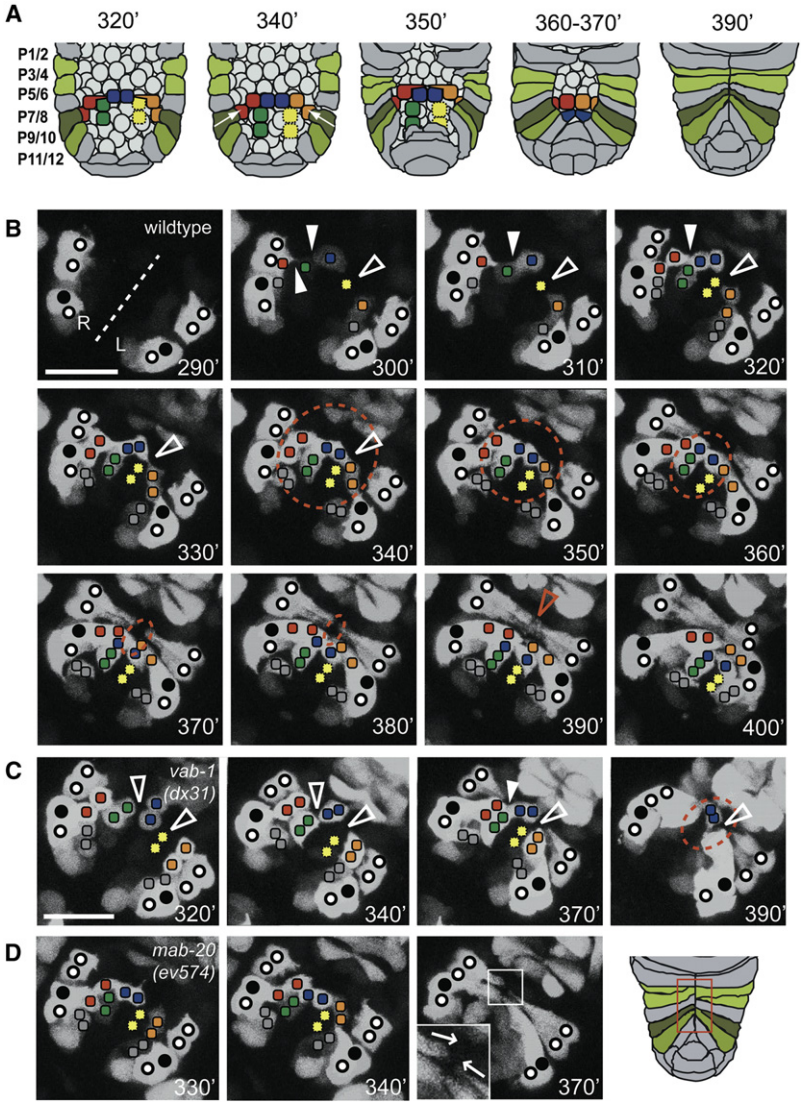

Figure 1. Pocket Bridge Formation and Pocket Closure in the Wild-Type and in *mab-20* and *vab-1* Mutants

(A) Schematic of epidermal pocket closure in minutes post-first cleavage (PFC) of the zygote. Ten plexin band cells span the open pocket. Cell births and movements were followed using *Pplx-2::gfp*. Plexin band cells of the same color are sisters. Rearrangement of plexin band cells during pocket closure is as photographed in (B).

(B) Ventral view of the pocket region of a wild-type embryo with anterior at top right. The ventral midline (dashed line) and relative positions of expressing identified P cells (circles, closed circles are P9/10) and plexin expressing cells on the surface of the open ventral pocket (colored squares) are indicated. Developmental time at 20°C is indicated in each frame. The approximate size of the open pocket (dashed circle) reflects the advance of P cell extension toward the midline. At 290′ PFC, *Pplx-2::gfp* is expressed in the P cells. At 300′–310′ PFC, blast cells on the surface of the open pocket express *Pplx-2::gfp*. At 320′–350′ PFC, expressing blast cells divide and sister cells remain attached to form a contiguous band of plexin expressing cells (plexin band), which spans the open pocket (when sporadically expressing yellow cells of Figure S1 are included). The midline distal pairs (red and orange squares) form the pocket bridge by migrating toward the midline over intervening expressing scaffold cells (green, yellow, and blue squares). This rearrangement requires protrusions from the presumptive bridge cells that extend over scaffold cells toward the ventral midline in two stages (330′ open arrowhead) (see summary in Figure 2). P9/10 cell migration then occurs along the forming and mature pocket bridge. At 390′ PFC, P cell migration stops when opposing leading edges meet at the midline. At 400′ PFC, contralateral marginal cells align and suture and the embryo begins to elongate and turn.

(C) Plexin band cells form a nearly contiguous band of cells by 340′ PFC in *vab-1(dx31)* null as well as in kinase dead embryos (data not shown). The nonsister cell gaps (left open arrowhead at 320′) are usually closed later by unknown mechanisms that might involve small filopodia-like projections (solid arrowhead at 370′).

(D) Skewed P cell leading edges (see 370′ inset) were detected in two of five *mab-20(ev574)* mutant embryos examined. Scale bar in (B) for (B)–(D) represents 10 μm.

closure in detail. We developed a variety of reporters for *vab-1* and *plx-2* expression (see Table S1 available online; Experimental Procedures). At the onset of pocket closure, the *plx-2* reporters express in right and left side analogs of QV5 and P cells P3/4, P5/6, P9/10, P11/12 (Figures 1, 2, and 3; Figure S1), whereas *vab-1* reporters express in right and left side analogs of V3 (sporadically), V4, QV5, and P9/10 (Figure 4). Both reporters also express in bridge and scaffold cells (see below), which together comprise a band of PLX-2 and VAB-1 expressing cells that cross the open pocket (brackets in Figures 3 and 4), referred to below as the plexin band. Expression in all of these cells continues throughout pocket closure and beyond. Among the P cells, expression is most prominent in P9/10 right (R) and left (L) for all reporters.

We used time-lapse analysis of a *plx-2::gfp* reporter to characterize cell divisions, movements, and associations involved in pocket closure (Figures 1, 2, and 3; Figure S1). The results presented below derive from time-lapse analysis of 20 wild-type, 14 *vab-1(dx31)* null, four *vab-1(e2)* kinase dead, and five *mab-20(ev574)* null mutant embryos and from visual inspection of dozens of embryos of each genotype by epifluorescence and differential interference contrast microscopy, which confirm the time-lapse findings.

At the onset of pocket closure, the *plx-2* reporter expresses in six blast cells (and sporadically in a seventh—see Figure S1C) on the surface of the open ventral pocket, five of which, after dividing, form a band of ten PLX-2/plexin expressing plexin band cells (Figures 1, 2, and 3; Figure S1C in which sister cells are denoted by the same color) that extends across the midline spanning the open pocket. Time-lapse analyses show that the plexin band cells are of two functional types. One type comprises three sister cell pairs—one roughly dorsal-ventral (D/V)-oriented midline proximal sister pair (born just right of the presumptive midline) whose border, following a slight rearrangement, comes to lay on the ventral midline (blue cells in Figures 1 and 2), plus flanking anterior-posterior (A/P)-oriented sister pairs on each side (yellow and green cells in Figures 1 and 2). These six cells rearrange slightly so that they span across the ventral midline and form a scaffold for movement of the other set of four cells (midline-distal red and orange sister pairs) toward the midline, where they form a single-cell-wide and -deep transverse

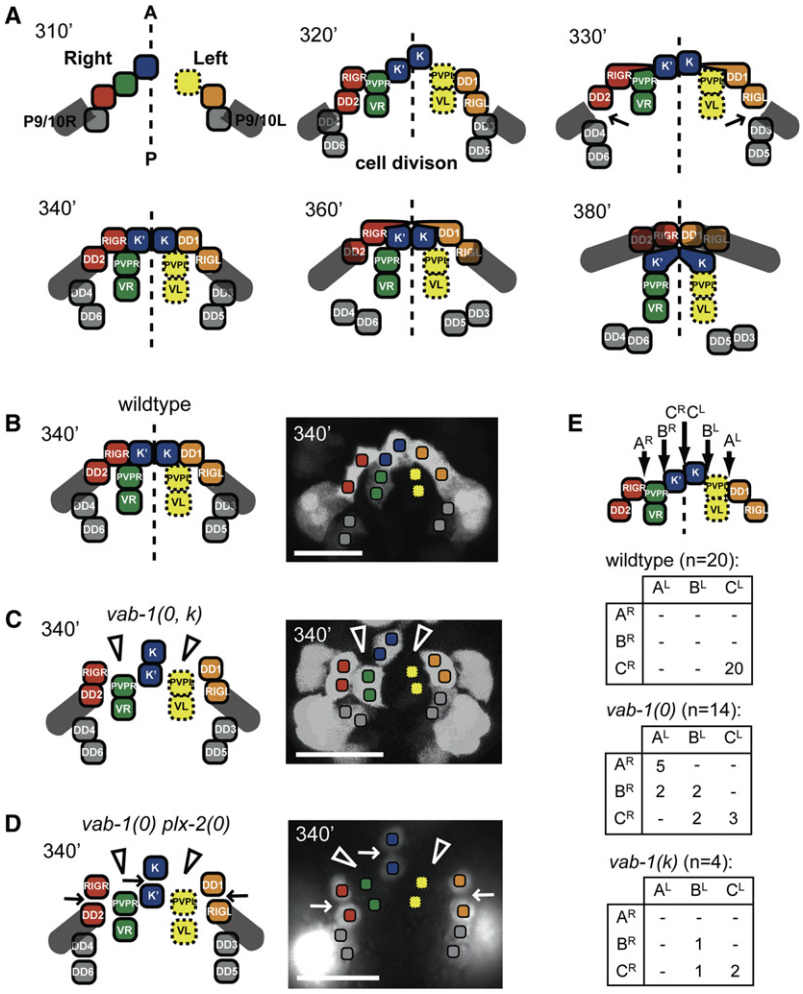

Figure 2. Schematic of Pocket Bridge Formation in the Wild-Type and Mutants

Relative stages of pocket bridge formation from plexin band cells are shown in minutes PFC using the *Pplx-2::gfp* reporter.

(A) Summarizes cell identities, bridge assembly, and P9/10 cell migration as derived from Figure 1, shown in Figure S2A, and described in the Results.

(B and C) In *vab-1* null and kinase dead mutants *(0, k)*, pocket bridge cells (red and orange) fail to form or maintain the directed protrusions (open arrowheads) required for their movement over the scaffold cells (green, blue, and yellow cells) to the midline. Pocket bridge formation at this time remains in an obstructed state.

(B and D) The plexin band is more severely disrupted in the *vab-1 plx-2* double null. Gaps are present between sister (arrows) and nonsister (open arrowheads) plexin band cells.

(E) P9/10 cells stop progression toward the midline at positions A, B, or C right (^{R}) or left (^{L}). The number of embryos with a particular position of blockage is shown as the intersection of a specific row (right side block) with a specific column (left side block). Scale bars represent 10 μm.

queue of *plx-2* and *vab-1* expressing cells on the surface of the open pocket. These four cells form a bridge that serves as a substratum for the migration of contralateral P9/10 cells to the midline.

Bridge Formation

Bridge assembly occurs with near left/right mirror-image symmetry. Each midline distal pair of bridge-forming cells on each side (red cell on the right and orange cells on the left in Figures 1 and 2A) must migrate over the scaffold cells to meet at the ventral midline. This occurs in phases. First, the anterior sister of each pair of presumptive bridge cells on each side extends a narrow protrusion over the anterior surface of the anterior sister of the adjacent scaffold sister cell pair (see Figure 1B, 320′ and 330′ arrowheads, and Figure 2A, 330′). This protrusion attaches to the border between scaffold cells (Figure 2A, red to blue and orange to blue cell borders) then retracts, pulling the attached presumptive sister bridge cells toward the site of attachment (Figure 2A, 330′–340′). This is repeated using the midline proximal scaffold cell as a substratum for protrusion and the border between midline straddling blue cells for attachment. Retraction then pulls the attached contralateral sister bridge cell pairs to the midline and aligns them along the D/V body wall axis to form the transverse pocket bridge (Figure 2A, 360′–380′), which spans the open ventral pocket from left to right margins. Coordinate with these movements is a general squeezing together of the two sides of the embryo.

P Cell Migration over the Pocket Bridge to the Ventral Midline

As the pocket bridge is assembling, the P9/10 cells begin to migrate over the presumptive bridge cells toward the ventral midline (Figure 1B). A translational reporter for PLX-2 is localized at the leading edge of these and other P cells during this time (Figures 3D–3F). Other P cells may initially contact the bridge cells (Figure 3D, inset) but lose contact when the leading edge of each P9/10 cell begins to migrate across the bridge while spanning its entire width (Figure 4I, closed arrowhead). When the P cells reach the midline, they stop, align with their contralateral partners, and seal the midline to complete pocket closure. The embryo then begins to turn, marking the onset of circumferential constriction of epidermis and embryo elongation.

Bridge Formation and P Cell Progression to the Midline in *vab-1* Mutants

Mutants of *vab-1* and *mab-20* are known to affect ventral pocket closure [6, 8]. Many *vab-1* null mutant [*vab-1(0)*] embryos fail to close the open ventral pocket before embryo elongation begins [8, 13]. The residual hole in the mutant epidermis provides a conduit for the extrusion of internal blast cells from the embryo, thereby causing lethality (Figure S2A). This closure defect identifies a role for VAB-1 in regulating the ability of the P cells to migrate to the ventral midline before embryo elongation occurs.

Although approximately 40% of *vab-1(0)* mutant embryos die by expelling inner embryonic cells through an open pocket (Figure 5C; Figure S2; Table S2; see also [8]) or in principle through a weakened midline that breaks open (see below), the remaining embryos successfully complete ventral pocket closure and survive. Among these, only mild misalignments of contralateral P cells occur at the ventral midline (Figures S3A–S3D; Table S2).

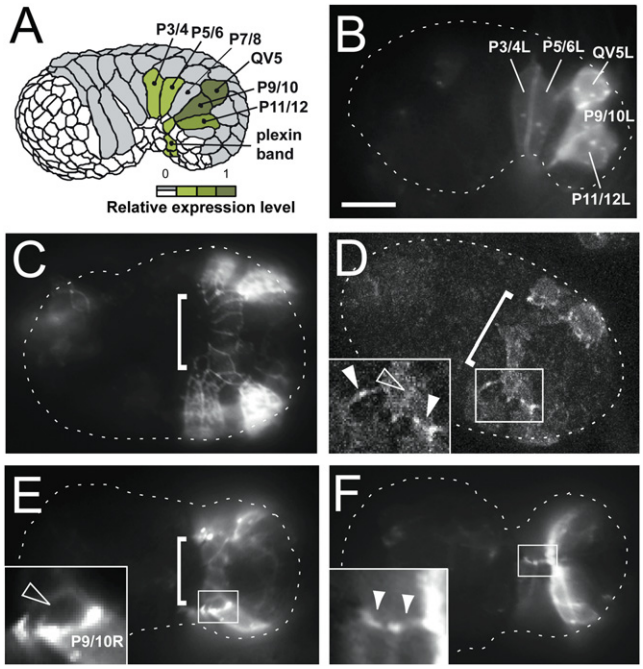

Figure 3. PLX-2 Is Expressed in the Plexin Band and P Cells Undergoing Pocket Closure

Fluorescence is from *Pplx-2::PLX-2::GFP* translational reporter. Anterior is to the left.

(A) Summary of *plx-2* reporter expressing (green) cells.

(B) Lateral view at the beginning of pocket closure. PLX-2::GFP is expressed in a subset of P cells at the margin of the open pocket.

(C) Ventral view at the onset of pocket closure showing PLX-2::GFP-expressing plexin band cells (bracket).

(D) Ventral view showing a confocal section of the ventral pocket. PLX-2::GFP is enriched at the leading end and filopodial-like tips of migrating P cells (solid arrowheads). Before the onset of pocket closure, P5/6 tips contact the plexin band (left arrowhead, inset) as do extensions from P9/10 (right arrowhead, inset).

(E) Ventral view showing the assembling bridge (bracket) and PLX-2::GFP-enriched P cell tips (also see inset).

(F) Ventral view showing PLX-2::GFP-enriched P cell tips (inset) as they meet at the ventral midline. Scale bar represents 10 μm.

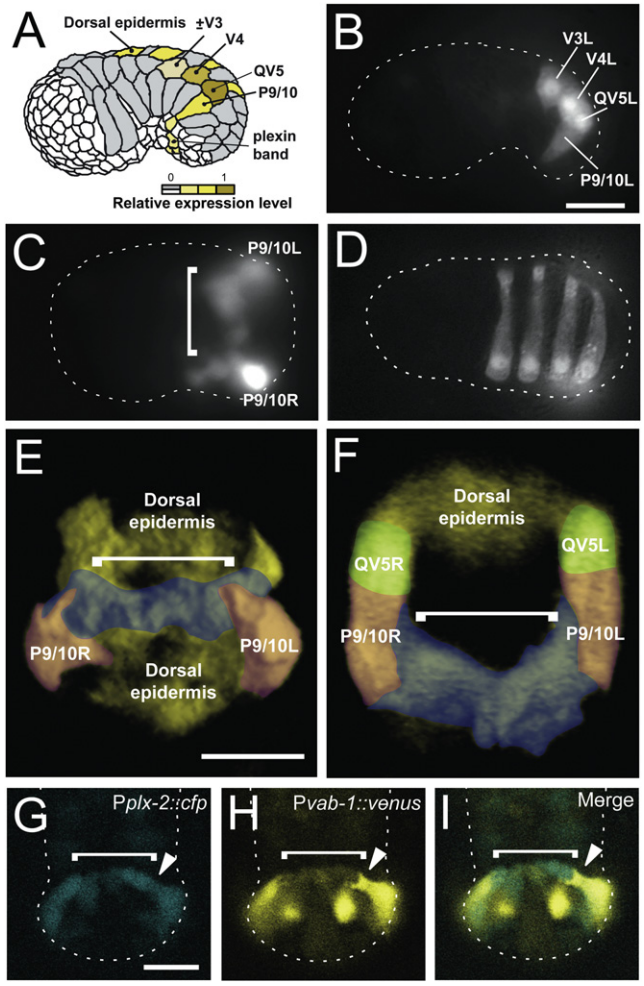

Figure 4. *vab-1* and *plx-2* are Coexpressed in P9/10 and the Plexin Band

(A–F) Fluorescence is from *Pvab-1::venus(yfp)* transcriptional reporter. Anterior is left unless stated otherwise.

(A) Summary of *vab-1* reporter expressing (yellow) cells.

(B) Lateral view. *vab-1* is expressed in V3, V4, and coexpressed with *plx-2* in QV5 and P9/10.

(C) Ventral view. *vab-1* is expressed in the plexin band of single cell width on the ventral surface of the open pocket (bracket) prior to P cell migration.

(D) Dorsal view. *vab-1* is expressed in alternating, left side posterior epidermoblasts overlying the enclosing pocket.

(E and F) Reconstructed three-dimensional ventral view (E) and cross-sectional view (F) from a stack of confocal images of *vab-1* expression during early pocket closure. False color was added to provide contrast. Differentially colored cell types are named except for the plexin band (blue), which is indicated by a bracket.

(G–I) Anterior is up. Confocal images of the *Pplx-2::cfp* reporter showing the pocket bridge (bracket) in (G) in direct contact with the migratory leading end of P9/10 (closed arrowhead) of *Pvab-1::venus* in (H). Merged image in (I) shows *plx-2* and *vab-1* reporter expression overlaps in P9/10 (closed arrowhead) and the pocket bridge (bracket) with P9/10 migrating on the pocket bridge. Scale bars represent 10 μm.

Eph receptors like VAB-1 can have both kinase-dependent and kinase-independent activities [14]. George et al. [8] previously found that P cell midline alignment and embryonic lethal defects are relatively rare in the kinase dead [*vab-1(e2)*] mutant embryos compared to *vab-1(0)* embryos (see also Figures 5A and 5C; Table S2), suggesting that a kinase-independent function of VAB-1 is largely sufficient for these processes.

To further examine the roles of Eph receptor and semaphorin signaling in pocket closure, we followed dozens of carefully staged embryos of *vab-1* null and kinase dead mutants and also analyzed null (n = 14) and kinase dead (n = 4) embryos by time-lapse photomicroscopy. The spatiotemporal pattern of *plx-2* expression revealed that the pocket bridge and scaffold progenitors, their subsequent divisions, and adhesion between sister cells appeared unaffected in all *vab-1* null and kinase dead embryos examined (Figures 1C and 2C; Figure S2). Reported gastrulation defects in *vab-1(0)* embryos [8] did not produce obvious disorganization of plexin band cells in any embryos we examined, possibly because embryos can correct or bypass these defects. However, we did find that none of the *vab-1(0)* or *vab-1(k)* mutant embryos was able to form or maintain the narrow bridge cell protrusions that normally extend over the anterior surface of the scaffold cells to pull the presumptive bridge cells to the midline. These protrusions were also never observed in the staged mutant embryos.

Although the absence of these protrusions is the likely cause of ventral pocket defects in *vab-1* null embryos, 97% of these also have gaps between nonsister plexin band cells beyond

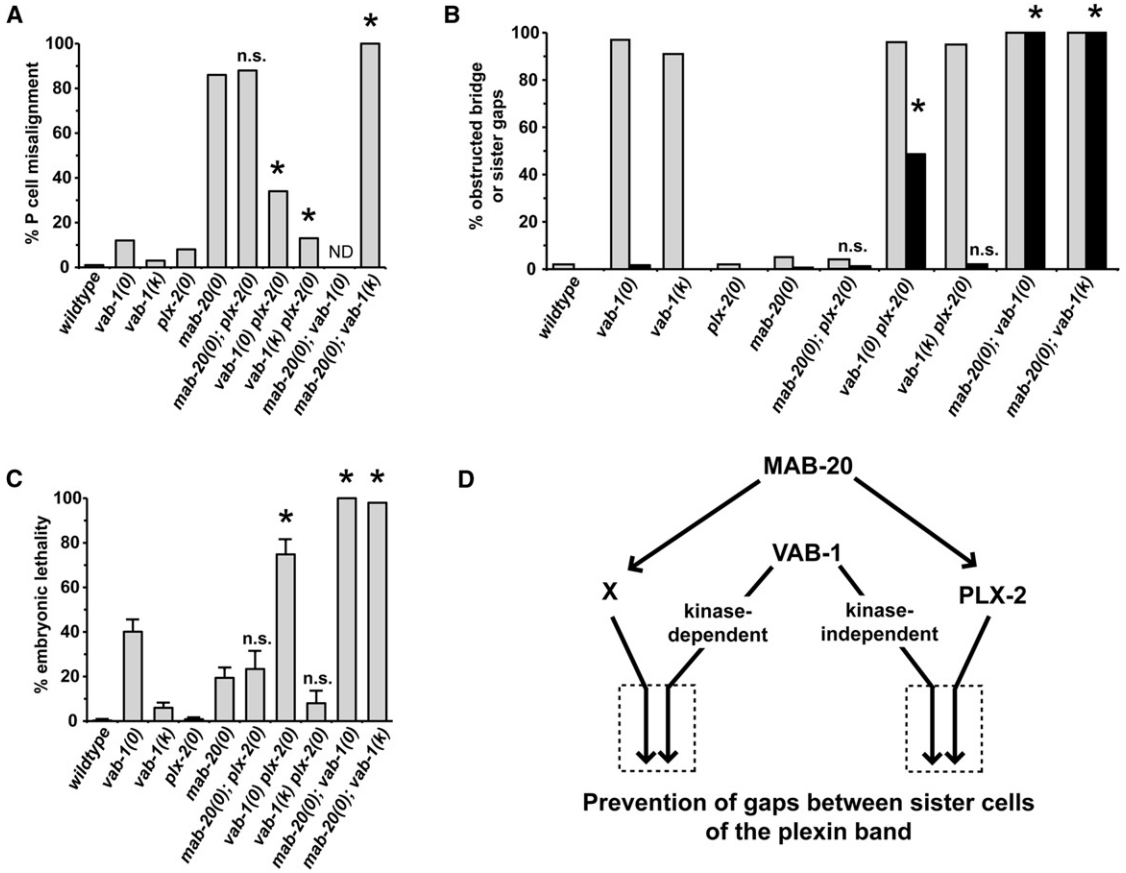

Figure 5. Analysis of P Cell Ventral Midline Alignment, Pocket Bridge Formation, and Embryonic Lethality in *vab-1*, *mab-20*, and *plx-2* Mutants

Data are from transgenic lines in Table S3.

(A–C) Genetic analyses utilized null mutants *vab-1(dx31)*, *mab-20(ev574)*, *plx-2(ev773)*, and kinase-dead mutant *(k) vab-1(e2)*. Strain *mIn1[mIs14 dpy-10(e128)]* (Edgley and Riddle, 2001), was used to balance the complete and nearly complete embryonic lethality of the *mab-20; vab-1(0)* and *mab-20; vab-1(k)* double mutants, respectively.

(A) The percentage of L1s with P cell ventral midline alignment defects was scored (n ranges from 121 to 173). The complete embryonic lethality of the *mab-20*; *vab-1(0)* precluded the analysis of midline defects (ND).

(B) The percentage of embryos with an obstructed bridge (gray bars) or gaps between sister plexin band cells (black bars) present at 340′ PFC are shown for wild-type and mutant animals (indicated on the abscissa). Because of *mab-20*; *vab-1* double mutant lethality, only 53 and 45 animals were scored from *mab-20; vab-1(0, k)* balanced lines, respectively. Essentially all *vab-1* null and *vab-1 plx-2* double null embryos also had gaps between nonsister plexin band cells.

(C) Embryonic lethality was scored as described in Experimental Procedures. Error bars represent SEM. Data presented without error bars represent a single sample of size n (see Table S2). Significant interactions (comparing double to single mutants) are shown with an asterisk. For (A) and (B), a two-sided Fisher's exact test was used, and for (C), an unpaired t test (two-tailed $p < 0.05$) was used to determine significance of interactions.

(D) Genetic model of semaphorin and Eph signaling during pocket closure. The penetrance of single and double mutant pocket closure defects indicate that MAB-20 signals through two mechanisms—PLX-2-dependent and PLX-2-independent mechanisms (the latter mediated by hypothetical receptor X). Double-mutant data suggest that the kinase-independent function of VAB-1 functions redundantly (boxed arrows to the right) with PLX-2, whereas the kinase-dependent function of VAB-1 functions redundantly (boxed arrows to the left) with unknown (X) to prevent the nonsister gaps and consequent embryonic lethality.

340′ post-first cleavage (PFC) of the zygote (Figure 1C, 340′; Figure 2C; Figure S2) when these gaps are usually closed in wild-type embryos (Figure 1B, 340′; Figure 2B). These gaps could, in principle, also be causal for embryonic lethality, however, in most null and kinase dead embryos, these gaps are closed with a delay (i.e., after 340′ PFC), possibly by small filopodia-like protrusions sometimes seen emanating from bridge and scaffold cells (Figure S2, 360′ closed arrowhead) or by constriction of the entire midline region. This suggests that these gaps delay rather than block pocket closure.

As a consequence of the protrusion defects or gaps between nonsister cells, the presumptive pocket bridge cells are impeded in their migration over the scaffold cells to reach the midline. The entire group of unrearranged cells caused by this defect is referred to hereafter as the "obstructed bridge" even though in many embryos it appears to assemble with a delay just in advance of P9/10 cell migration (see below).

An obstructed pocket bridge variably hindered progression of P9/10 cells toward the midline (Figures 2C and 2E). In some *vab-1* mutant embryos, P9/10 cells progressed minimally toward the ventral midline. In these cases, blocks in P9/10 migration often occurred at borders between scaffold cells (Figure 2E). In other embryos there was substantial progression of P9/10 cells toward the midline, but this was slower than in wild-type embryos and involved movement of the entire leading edge of the presumptive bridge cells toward the midline just in advance of the P9/10 leading edge (see Discussion).

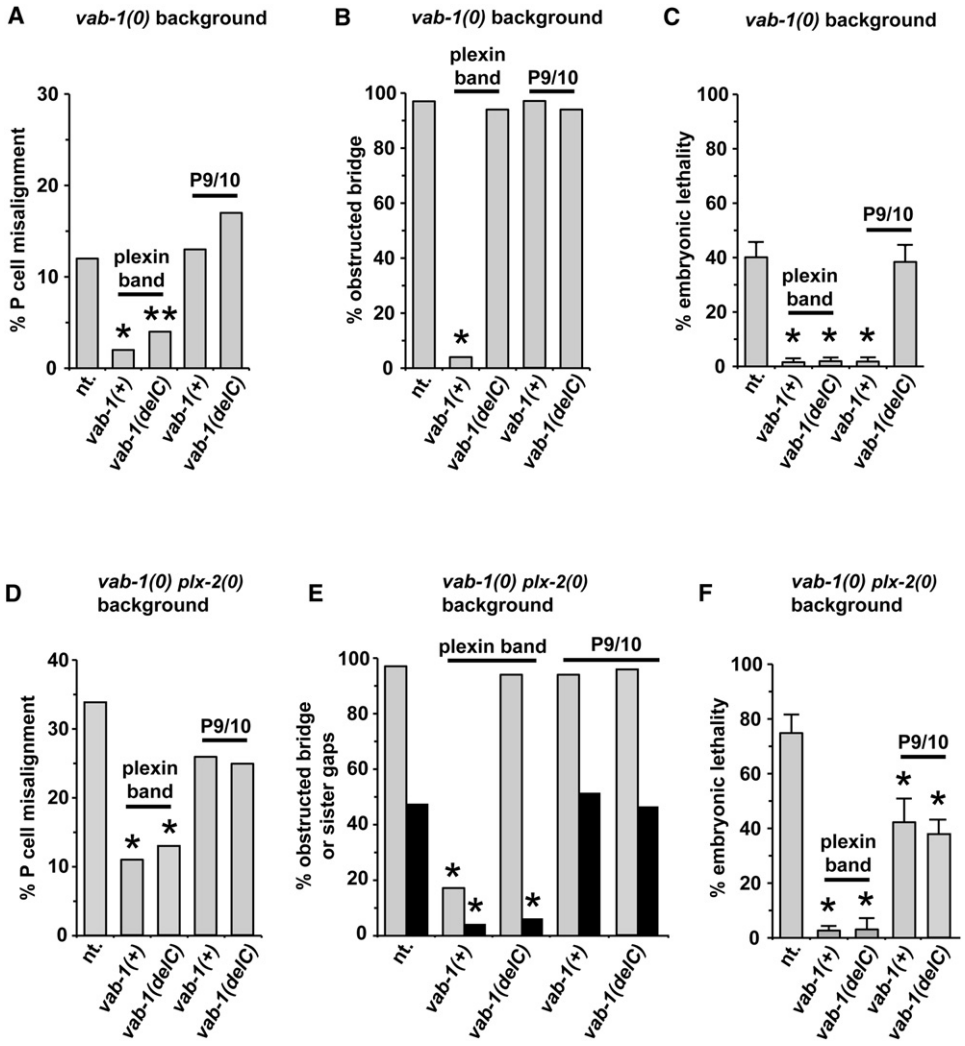

Figure 6. Cell-Specific Rescue of *vab-1* Null and *vab-1 plx-2* Double Null Mutant Embryos by *vab-1(+)* or *vab-1(delC)*

Data are from highlighted transgenic lines in Table S3. Shown are the fractions of embryos with P cell midline ventral alignment defects (A and D), with an obstructed bridge (gray bars) or with gaps between sister plexin band cells (black bars) at 340′ PFC (B and E), and that die as embryos from an open pocket defect (C and F), for *vab-1* null mutant animals (A–C) or for *vab-1 plx-2* double null mutant animals (D–F) that carry no *vab-1* transgene (abbreviated nt. on abscissa) or carry the transgene indicated on the abscissa expressed by the cell type indicated above the data bars. Error bars represent SEM. Data presented without error bars represent a single sample of size n (see Table S3).

Five of eight P9/10 cells in kinase dead embryos and only eight of 28 in null embryos reached the midline before embryo elongation began. There were also few, if any, kinase dead embryos in which a P9/10 cell failed to migrate at all or migrated minimally toward the midline (0 of 8 compared to 12 of 28 for null embryos). Among the types of mutant embryos observed, only those in which both P9/10 cells fail to migrate (5 of 14 null and 0 of 4 kinase dead) have a severe open pocket defect at the time embryo elongation begins, whereas others have a small open pocket defect (Figure 2E). These results suggest that the ability of P9/10 cells to migrate over an obstructed pocket bridge is efficient enough in *vab-1* null embryos to account for their 60% embryonic viability but even more efficient in *vab-1* kinase dead embryos accounting for their 94% viability.

Cell-Type-Specific Rescue of P Cell Midline Alignment Defects of the *vab-1* Null Mutant

We sought to distinguish a P cell midline alignment function for the VAB-1 kinase and extracellular domains in plexin expressing band cells and P9/10 cells (Figure 6). We did this by first identifying *plx-2* regulatory sequences able to drive expression of GFP (Figure S4) in the plexin band or separately in P9/10. Using these promoters to drive *vab-1*expression, we found that P9/10 cell expressed *vab-1(+)* does not rescue P cell midline alignment defects of the *vab-1* null whereas plexin band expressed *vab-1(+)* or *vab-1(delC)* does rescue (Table S3). These results demonstrate that the VAB-1 extracellular domain on the surface of plexin band cells can mediate P cell midline alignment even in the presence of an obstructed pocket bridge. This is consistent with the ability of wild-type and kinase dead alleles to mediate normal P cell alignment.

PLX-2 and MAB-20 Function in P Cell Guidance and Alignment

The penetrance of *mab-20* and *plx-2* null mutant P cell midline alignment defects are 86% and 8%, respectively (Figure 5A; Table S2). *mab-20(0)* and *plx-2(0)* embryos do not have obvious open pocket defects, yet *mab-20(0)* embryos extrude

internal cells from the ventral side [6] suggesting that severe P cell alignment defects weaken the midline, causing it to rupture when circumferential constrictive forces of embryo elongation occur.

Despite more severe (Figures S3A–S3D) and eight times more penetrant midline alignment defects in the *mab-20* null (Figure 5; Figures S3A–S3D; Table S2), the penetrance of lethality among *mab-20(0)* embryos is significantly lower than for *vab-1(0)* embryos (Figure 5C). These data suggest that the P cell alignment defects per se do not contribute significantly to *vab-1(0)* mutant lethality; instead, the lethality results from a more severe effect on pocket closure, including failure of P cells to migrate sufficiently to the midline before embryo elongation occurs or failure to form a proper midline seal.

The *plx-2(0)* mutation was unable to significantly enhance either the P cell midline alignment defect or the embryonic lethality of the *mab-20* null (Figures 5A and 5C). This is consistent with PLX-2 acting in the same pathway as MAB-20 to prevent these two defects and with the finding by Nakao et al. [7], that MAB-20 binds PLX-2. The greater lethality and P cell alignment defects of the *mab-20(0)* suggest that MAB-20 also functions through at least one PLX-2-independent pathway to prevent the two defects (Figure 5D). LAD-2 is another reported receptor for MAB-20 that could mediate the PLX-2-independent functions of MAB-20 [12]. We examined *lad-2* mutants and doubles of *lad-2* with the *plx-2*, *mab-20*, and *vab-1* mutant alleles and found very little lethality or enhancement of lethality in any of these strains (Figure S3E), ruling out LAD-2 as an important component of ventral enclosure.

Two of five *mab-20(0)* embryos exhibited a detectable skewing of the P cell leading edges from the D/V body wall axis as they migrate toward the midline (Figure 1D, 370′ inset), not observed in the wild-type (n = 20). In contrast to *vab-1* mutants, none of the *mab-20* embryos showed a significant delay in either the onset or the rate of P cell migration (n = 5). For this reason we suggest that P cell misalignment in *mab-20* and *plx-2* mutants is caused by a defect in P cell polarity or guidance, or abnormal adhesions of P cell leading tips, but not by a defect in P cell progression toward the midline.

Cell-Type-Specific Rescue of Pocket Closure and P9/10 Cell Migration over an Obstructed *vab-1* Mutant Pocket Bridge

We also used the *plx-2* regulatory regions to drive *vab-1(+)* or *vab-1(delC)* expression in the plexin band cells or in P9/10 to determine in which cell type the expression of each gene is able to rescue (1) *vab-1* null mutant pocket bridge formation, and (2) the ability of P9/10 to migrate over an obstructed bridge (as measured by prevention of embryonic lethality). At one extreme, P9/10 cell expression of *vab-1(delC)* did not rescue any of the pocket closure defects of the *vab-1* null, and at the other extreme, plexin band expression of *vab-1(+)* rescued all pocket closure defects of the *vab-1* null including formation of an unobstructed bridge and P cell alignment (Figures 6A–6C; Table S3). The latter finding is consistent with a requirement for VAB-1 kinase activity in either the bridge or scaffold cells to extend or maintain the narrow protrusions required for pocket bridge assembly.

Although pocket bridge formation was not significantly rescued by P9/10 expression of *vab-1(+)*, this expression was able to rescue the embryonic lethality of the *vab-1* null, as was plexin band expression of *vab-1(+)* or *vab-1(delC)* (Figure 6C; Table S3) by facilitating P9/10 cell migration over an obstructed bridge. Thus, *vab-1(+)* activity in P9/10 cells appears to be equivalent to *vab-1(delC)* or *vab-1(+)* activity in the plexin band in rescuing pocket closure defects. This raises the possibility that reverse signaling from VAB-1(delC) on the plexin band to P9/10 cells and forward signaling from the plexin band to VAB-1(+) on the P9/10 cells are equivalent in their ability to facilitate P cell migration over an obstructed pocket bridge, although other explanations are also feasible (see Discussion).

PLX-2 and VAB-1 Function Redundantly to Prevent "Gaps" between Sister Plexin Band Cells

VAB-1 and PLX-2 appear to have distinct functions in ventral enclosure. For example, unlike *vab-1* mutations, *plx-2* and *mab-20* mutations do not affect pocket bridge formation or the rate of P cell migration to the midline. However, we did observe some unexpected genetic enhancement of embryonic lethality caused by pocket closure defects in *vab-1 plx-2* and *mab-20; vab-1* double null mutants.

There are at least three patterns of enhancement possible in double mutants. Additive enhancement of a specific defect shared by mutants of two genes (when both cause a loss of function and at least one is a null) suggests that the two genes function in parallel to prevent the defect. Synergistic enhancement by mutants of two genes suggests that the genes may also function partially redundantly to prevent the defect. Synthetic defects are an extreme version of synergistic enhancement that occurs when a defect manifests in the double that was not obvious in either single mutant. This usually indicates that function of each gene is entirely redundant with the other, especially if the defect is specific, unlike a poorly defined defect such as "lethality" or "sterility."

A block or delay in bridge assembly, causing an obstructed bridge, occurs in over 90% of *vab-1* null and kinase dead embryos (Figure 5B; Figure S2; Table S2), so enhancement by *plx-2* or *mab-20* mutations cannot be determined accurately for this phenotype. However, the few P cell alignment defects of the *vab-1* kinase dead mutant are enhanced additively by *plx-2* and synergistically by *mab-20* null mutations, whereas the alignment defects of the *vab-1* null are enhanced largely additively by the *plx-2* null (Figure 5A). These results suggest that the kinase and nonkinase functions of VAB-1 act in a molecular pathway that functions largely in parallel with the PLX-2 pathway, whereas VAB-1 acts redundantly with MAB-20 to regulate P cell alignment.

The genetic interactions of *plx-2* and *mab-20* with *vab-1* mutations in preventing pocket closure defects are more complex. For example, the *vab-1* null mutation enhances both the *plx-2* null and the *mab-20* null synergistically for embryonic lethality (this enhancement is largely synthetic) (Figure 5C). By contrast, the kinase-deficient *vab-1(e2)* mutation enhances the embryonic lethality of the *plx-2* null additively, if at all (Figure 5C), but enhances the *mab-20* null synergistically. These results suggest that the kinase function of VAB-1 is redundant with the PLX-2-independent function of MAB-20, and the kinase-independent function of VAB-1 is redundant with the PLX-2-dependent function of MAB-20 in preventing pocket closure defects (see Figure 5D and Discussion).

All plexin band cells (i.e., bridge plus scaffold cells) are present in roughly normal positions in the *vab-1 plx-2* double null mutant embryos. However, time-lapse analysis shows that double mutant embryos unexpectedly have narrow gaps between sister plexin band cells (hereafter referred to as sister

cell gaps) that are not present in the *vab-1* null or the wild-type (see Figure 2D, 340′) in addition to the gaps between nonsister plexin band cells that are found in 97% of *vab-1* null embryos. The gaps between sister plexin band cells in the *vab-1 plx-2* double null are not as severe as in the *mab-20; vab-1* double null because the former have some aggregates of sister cells that are absent in the latter (data not shown). These results suggest that PLX-2 and MAB-20 have redundant functions with VAB-1 in forming or maintaining adhesions between sister plexin band cells, just as they have redundant functions with VAB-1 in preventing embryonic lethality.

The pattern of redundancies governing prevention of lethality (last four gray data bars to the right in Figure 5C) is nearly identical to the pattern of redundancies governing the prevention of gaps between sister plexin band cells (last four black data bars to the right in Figure 5B). This strongly suggests that the synergistic enhancement of *vab-1* mutant embryonic lethality by *plx-2* mutations is caused by the persistence of gaps between sister plexin band cells, which block migrating P9/10 cells from completing pocket closure. This interpretation is supported by cell-type-specific rescue data presented below and considered further in the Discussion.

Cell-Type-Specific Rescue of the *vab-1 plx-2* Double Null Mutant Pocket Closure Phenotypes

There are two obvious contributions to embryonic lethality of the *vab-1 plx-2* double null. One is the presence of gaps between sister bridge and scaffold cells, which (unlike gaps between nonsister cells) appear to perdure and block P cell progression to the midline. The other is the impeded ability of P9/10 cells to migrate over an obstructed pocket bridge caused by a *vab-1* deficit. We determined the degree of rescue of each of the *vab-1 plx-2* double null ventral enclosure phenotypes by plexin band or P9/10 expressed *vab-1(+)* or *vab-1(delC)* just as we did for the *vab-1* single null. The obstructed bridge phenotype of the double is rescued by plexin band expressed *vab-1(+)*, but not by the other three expression constructs (Figure 6E). This is precisely what was found for rescue of the *vab-1* single null (Figure 6B). Double-mutant gaps between sister plexin band cells were rescued by expression of *vab-1(+)* or *vab-1(delC)* in the plexin band, but not by either P9/10-specific expression construct (Figure 6E). This suggests that gaps between sister plexin band cells may normally be prevented by an adhesive function between these cells provided by the VAB-1 extracellular domain, although kinase-independent signaling through the largely resected cytoplasmic domain of VAB-1(delC) cannot be ruled out.

With one exception, the cell-type-specific rescue results for the *vab-1 plx-2* double-mutant defects are as expected based on the rescue of the *vab-1* single null using the same transgene arrays. The exception is P9/10 expressed *vab-1(delC)*, which does not rescue lethality of the *vab-1* single null (Figure 6C) but unexpectedly does partially rescue the lethality of the double null caused by an obstructed pocket bridge (Figure 6F). A plausible explanation for this result is presented in the Discussion.

Discussion

Formation of the Pocket Bridge

In the last phase of epiboly in *C. elegans*, there is a hole or open pocket in the ventral epidermis that must be closed before embryo elongation begins. Epidermoblasts that line this open pocket, called P cells, mediate pocket closure by migrating to the ventral midline where they align with their contralateral analogs and form adherens junctions with them to seal the embryo in epidermis. Our data show that contralateral P cell analogs P9/10 right (R) and P9/10 left (L) can play a primary regulatory role in the pocket closure process by migrating directly toward the midline on a queue of four *plx-2* and *vab-1* expressing neuron cell bodies that comprise a bridge that spans the width of the open pocket.

The pocket bridge forms from the two most lateral (on each side) of a total of five sister pairs of *plx-2* expressing cells that form a contiguous band of cells (the plexin band) that also spans the open pocket (Figures 1, 2, 3, and 4; Figure S1). All of these cells except the midline scaffold pair are neurons (Figure S1C), which later extend axons along the A/P body axis. How these neurons make the transition from extending a protrusion along the D/V axis to extending an axon along the A/P axis is unknown but may depend on signals from the ventral epidermis, which they previously helped to organize.

Pocket bridge assembly involves formation of narrow protrusions by the most anterior of the sister pair of presumptive bridge cells on each side. These protrusions extend over scaffold cells and then pull the anterior bridge cell and its attached sister toward the midline. *vab-1* null and kinase dead mutants fail to form or maintain these protrusions, leaving the pocket bridge in an unassembled, obstructed state. The exclusive rescue of presumptive bridge cell protrusions by plexin band expressed *vab-1(+)* suggests that these protrusions require VAB-1 kinase function in the bridge cells or nonautonomously in the scaffold cells. Lacking appropriate promoters to test this, it remains possible that "guidance" cue(s) for bridge cell rearrangements act directly through VAB-1 on the bridge cell surface.

Migration of P9/10 cells across the obstructed pocket bridge still occurs in *vab-1* mutants but is slower than movement across a mature pocket bridge. This movement does not involve the formation of distinct cellular protrusions but rather appears to involve movement of the entire leading edge of the presumptive bridge cells in advance of the leading edge of the P9/10 cell by unknown molecular mechanisms such that P9/10 may not contact the scaffold cells. *vab-1* null embryos are slower in this movement than kinase dead embryos, accounting for the finding that 40% of the null and only 6% of the kinase dead embryos have an open pocket at the time embryo elongation occurs. During migration over an obstructed bridge, there is a tendency for P9/10 cells to become delayed or blocked at one of two positions on each side that correspond to the normal positions at which presumptive bridge cell protrusions are formed (Figure 2E). This raises the possibility that the hesitation at these positions is caused by the same signals needed to initiate the extension or retraction of these protrusions.

When both P9/10 cells become persistently blocked at the midline-distal positions, this creates a large open pocket, whereas other blocks create a subtle open pocket defect (Figure 2E). For technical reasons, we were unable to follow these embryos during embryo elongation, so we could not determine which of the time-lapsed embryos extruded cells from their open pocket and died. However, five of 14 (36%) of the mutant embryos appeared blocked with a large open pocket, which is roughly equal to the known penetrance of *vab-1* null mutant embryonic lethality (40%). This is consistent with the idea that most embryos with large open pockets die and shows that some embryos with subtly open pockets are likely to survive their pocket defects.

VAB-1 Kinase Function in P9/10 Can Facilitate Its Migration over an Obstructed Bridge

VAB-1 kinase activity has two important cell-type-specific functions. As described above, VAB-1 kinase function in the plexin band is required for normal bridge formation. However, P9/10 migration over an obstructed bridge (caused by a *vab-1* null mutant defect) can be rescued by P9/10 expressed *vab-1(+)* (which rescues the narrow protrusions required for bridge formation) or by plexin band expressed *vab-1(delC)*. The latter rescue cannot be explained by rescue of bridge cell protrusions, but it could be explained by any of at least three molecular mechanisms that could facilitate P9/10 migration over an obstructed bridge. One is that VAB-1(delC) (which retains an 87 residue juxtamembrane domain that could be involved) is activated by an unknown ligand to transduce a signal in the plexin band cells that makes them a better substratum for P cell migration. A second is that the VAB-1 extracellular domain on the plexin band simply provides a change in adhesive function. A third possibility is that signaling from VAB-1(delC) on the plexin band to P9/10 (probably to an ephrin on P9/10) is equivalent to the forward signaling from an unknown ligand to VAB-1(+) on P9/10. The last possibility raises the speculation that the signal transduction mechanism activated by forward signaling from an ephrin (presumably on bridge cells) through VAB-1 kinase on the P9/10 cells could be functionally equivalent to the signal transduction cascade activated by reverse signaling of the VAB-1 extracellular domain on the bridge cells to an ephrin on P9/10. Examination of the role of cell-type-specific expression of various ephrins in P cell motility and ventral enclosure will be required to shed light on these models.

P Cell Alignment Is Nonautonomously Regulated by the VAB-1 Extracellular Domain on Plexin Band Cells

The difference between the penetrance of P cell midline alignment defects in *vab-1* null and kinase dead embryos raises the simple expectation that the VAB-1 extracellular domain mediates interactions between contralateral P cell partners that cause alignment. However, this is surprisingly not the case because only plexin band expression of *vab-1(+)* or *vab-1(delC)* rescues the P cell alignment defects of a *vab-1* null, whereas P9/10 expression of either form of *vab-1* does not.

Plexin band expressed *vab-1(+)* and *vab-1(delC)* also rescue pocket closure defects, raising the possibility that closure defects are causal for the alignment defects of a *vab-1* null. This is unlikely because there are arrays that rescue pocket closure, as measured by embryonic lethality, but do not rescue alignment (Figures 6A–6C). These results suggest that P cell alignment requires the VAB-1 extracellular domain, nonautonomously, on the plexin band and that misalignments in *vab-1* null embryos are not caused by migration over an obstructed pocket bridge (which happens in null and kinase dead mutants) or by impeded pocket closure per se. In principle, the VAB-1 extracellular domain on the plexin band cells may signal to P9/10 cells or mediate an adhesion between these two cell types for P cell alignment.

P9/10 Cells as Primary Regulators of P Cell Migration to the Midline

vab-1 mutant defects in bridge formation not only severely hinder P9/10 but also P3/4 and P5/6 migration to the ventral midline. Furthermore, any cell-type-specific rescue of a *vab-1* mutant that facilitates P9/10 migration to the midline also facilitates the migration of other P cells to the midline, including expression of *vab-1(+)* in P9/10. These results suggest that expression in P9/10 is sufficient to rescue migration of other P cells to the midline but may not be unique in this respect.

It is possible that coordinate blockage and rescue of neighboring P cell migrations to the midline requires their attachment to one another via, for example, the actin cable at the leading edge of the P cells [15]. By this model, other P cells would be pulled to the midline by P9/10, but once in the vicinity of the midline, their leading tips might be able to independently find and attach but not necessarily align to contralateral P cells. This would explain why late blocks in P9/10 cell migration do not affect the ability of P3/4 or P5/6 cells to reach the midline, whereas early blocks do.

P9/10 cells also appear to play a central regulatory role in P cell alignment at the midline because plexin band expressed *vab-1(delC)* nonautonomously rescues P cell alignment defects along the entire midline axis even though only P9/10 have intimate contact with the obstructed pocket bridge in a *vab-1* null. This suggests that tracking of P9/10 along even an obstructed pocket bridge can keep all the P cells in correct register with one another and cause them to align at the midline.

Semaphorin-2a/mab-20 Mutations Cause Defects in the Guidance of the Leading Edge of P Cells

PLX-2 clearly functions in the same pathway as MAB-20 for pocket closure [7]. The milder and less penetrant effect of the *plx-2* null compared to a *mab-20* null suggests that MAB-20 plays an additional PLX-2-independent role in pocket closure, as in male ray cell sorting [16]. Our results suggest that MAB-20 and PLX-2 affect P cell midline alignment by a different mechanism than VAB-1. Nevertheless, the more than additive penetrance of the *vab-1 plx-2* double null mutant suggests that semaphorin and Eph receptor signaling have parallel and possibly partially redundant functions in the alignment process.

VAB-1 Has a Redundant Function with PLX-2 in Regulating Sister Plexin Band Cell Adhesions and a Nonredundant Function in Facilitating P9/10 Cell Migration over an Obstructed Pocket Bridge

There are two contributions to open pocket defects and consequent embryonic lethality in *vab-1 plx-2* double mutants. One comes from the gaps that are present between sister plexin band cells. This defect, which has a penetrance of 48%, depends on a deficiency in both *vab-1* and *plx-2* function. Another contribution to double mutant lethality is the reduced ability of P9/10 to migrate over an obstructed pocket bridge. Although this defect can clearly be caused by a deficiency in *vab-1* function alone, in principle, the *plx-2* mutation in the double could further reduce the ability of P9/10 to migrate over an obstructed bridge. If there were no effect of the *plx-2* mutation on migration over the double-mutant obstructed bridge, this would predict that lethality would occur in all 48% of embryos with sister cell gaps plus 40% of those embryos without sister cell gaps (or 40% of 52% = 21%) or a total of 69% lethality for double mutant embryos, which is not significantly different from the observed lethality of 75% (Figure 5C; Table S2). Thus in the double mutant, sister cell gaps prevent P9/10 progression to the ventral midline; however, a *plx-2* deficit in embryos without sister cell gaps does not further hinder P9/10 progression over an obstructed bridge, but rather this hindrance results from the *vab-1* deficit

alone. However, because the penetrance of obstructed bridges is nearly 100% in these double mutants, the sister cell gaps are almost never present alone; therefore, we cannot yet be certain whether the sister cell gaps alone cause open pocket defects or whether they do so only in combination with an obstructed bridge.

These two contributions to lethality in *vab-1 plx-2* double-mutant embryos represent two separable functions of VAB-1 as determined by cell-specific rescue experiments. For example, as described above, the inability of P9/10 to migrate over an obstructed bridge can be rescued by *vab-1(+)* or *vab-1(delC)* expressed in either P9/10 or plexin band cells, respectively. In contrast, only plexin band expressed *vab-1(+)* or *vab-1(delC)* can prevent sister plexin band cell gaps. This likely reflects a redundant adhesive function of the VAB-1 extracellular domain on the surface of the plexin band with PLX-2. In the future it will be interesting to determine whether the site of redundant PLX-2 function in preventing sister cell gaps is also on the surface of the pocket bridge.

Remarkably, the synergistic interactions identified by double-mutant phenotypes are complex (Figure 5D). These results suggest that MAB-20 has PLX-2-independent functions that are redundant with the kinase activity of VAB-1, whereas its PLX-2-dependent functions are redundant with a nonkinase activity of VAB-1 to prevent the extra lethality observed in the *vab-1 plx-2* double mutant caused by sister plexin band cell gaps. This is probably also the case for the redundancy of the VAB-1 kinase with the PLX-2-independent function of MAB-20 because the *mab-20; vab-1* doubles are fully penetrant for gaps between sister plexin band cells. This complex pattern of redundancy highlights the utility of genetics in elucidating redundancies that might otherwise go unnoticed.

PLX-2 May Normally Inhibit a Component of the VAB-1 Signaling Cascade in the P Cells to Regulate Pocket Closure

With one exception, all of the *vab-1 plx-2* double-mutant rescue results are completely consistent with expectations based on what is known about the nonredundant and *plx-2*-redundant functions of *vab-1* in pocket closure. The exception is the finding that P9/10 expressed *vab-1(delC)* can partially rescue the embryonic lethality of the double null that is caused by a putative deficit in P cell motility over an obstructed bridge even though it is totally incapable of rescuing any ventral enclosure phenotype of the *vab-1* single null. This suggests that loss of PLX-2 function somehow allows a function of VAB-1(delC) to compensate for loss of its cytodomain (e.g., kinase) activity. Such compensation could occur if, for example, PLX-2 normally antagonizes a function that is mediated by VAB-1(delC). Whether this or other molecular mechanisms are responsible for the unexpected rescue of the double mutant are important questions for future study.

Conclusions

Several features of ventral enclosure were identified in these studies, including the sorting of cells by VAB-1-dependent protrusions and the redundant function of PLX-2/plexin and VAB-1/Eph receptors in regulating adhesion between sister plexin band cells to assemble a bridge of cells that serves as a substratum for P9/10 cell movements to the ventral midline. Entirely unexpected was the finding that the VAB-1 extracellular domain works from the surface of the underlying plexin band cells to mediate P cell alignment because one might predict that a simple adhesive mechanism between contralateral P cell partners could suffice. A second unexpected finding is that P cell migration can occur over an obstructed bridge, presumably as a fail-safe process. Surprisingly, this can be facilitated by another VAB-1 function independent of its bridge-forming function. VAB-1 can enhance migration of P9/10 cells over an obstructed bridge in two different ways, one involving forward signaling from plexin band cells to P9/10 and the other involving kinase-independent signaling (possibly reverse signaling from plexin band to P9/10 or kinase-independent forward signaling from P9/10 to the plexin band). P9/10 cells can play a central regulatory role in basically all aspects of pocket closure as evidenced by cell-type-specific rescue results that are not attributable to the direct rescue of other P cells. Together, these findings may represent a new basis for understanding body wall closure in mammals, which, like *C. elegans*, use Eph receptor signaling [4, 5].

Experimental Procedures

Caenorhabditis elegans Strains and Maintenance

Bristol strain was grown at 20°C and cultured as described previously [17]. The following genes and alleles were used in this study: LG I: *mab-20(ev574)*; LG II: *lin-7(e1413)*, *vab-1(dx31)*, *vab-1(e2)*, *plx-2(ev773)*, *mIn1[mIs14 dpy-10(e128)]* (Edgley and Riddle, 2001); LG VI: *jcIs1[AJM-1::GFP]* [18].

DNA Constructs

plx-2 and *vab-1* expression constructs were used to make the following transgene arrays: *evIs190[Pvab-1::venus; pRF4]*; *evIs168[PLX-2::GFP; pRF4]*; *evIs136[Pplx-2::gfp; pRF4]*; and *evIs191[Pplx-2::cfp; pRF4]* (summarized in Table S1). *pRF4* encodes the dominant *rol-6(su1006)* cotransformation marker. Table S4 summarizes the derivation of constructs and corresponding transgene arrays used to identify *plx-2* promoter regions to drive P9/10 and plexin band specific expression. Table S5 summarizes the constructs that use these promoter regions to test cell-type-specific rescue of mutant embryos.

Double-Mutant Constructs

Multiple mutant strains were constructed by standard methods (Brenner, 1974). The *plx-2(ev773)* null mutation was passed into various strains using closely linked *lin-7(e1413)* as a balancer. A PCR assay was used to confirm the homozygosity of the *plx-2(ev773)* deletion.

Imaging and Time-Lapse Photomicroscopy

Gravid hermaphrodites were cut transversely through the vulva. Extruded embryos were mounted on 2% agarose pads in M9 solution. Transgenic reporters were observed by epifluorescence using a Leica DMRA2 microscope. Images were captured using a Hamamatsu camera and OpenLab software. Time-lapse imaging of embryos employed multiphoton laser scanning microscopy using a SpectraPhysics Ti:Sapphire laser tuned to 900 nm as described previously [19]. Data acquisition and stereo-4D processing were performed as described in [20]. Expressing cells were identified by following division patterns, timing, and position by time-lapse relative to the reported cell lineage [21].

Embryonic Lethality Assays

Individual L4 larval stage animals were allowed to develop and lay eggs under standard growth conditions at 20°C until egg-laying ceased. Lethality was determined by counting hatched and unhatched eggs. Ten to 14 broods were followed for each genotype.

Statistical Analyses

Embryonic lethality was expressed as a mean of a sample proportion of n broods of a single genotype and assumed to follow a binomial distribution. The confidence interval for the mean value was estimated as the SEM and is shown in Figures 5 and 6 by the error bars. To test for significant genetic interactions in embryonic lethality, we used an unpaired t test because these values represent continuous variable data. To test for significant genetic interactions for P cell alignment and pocket bridge defects, we used a two-sided Fisher's exact test utilizing a 2 × 2 contingency table

because these values represent categorical data (absence versus presence of defect). For all tests, a two-tailed p value of 0.05 was used as the cutoff for statistical significance ($p < 0.05$).

Supplemental Information

Supplemental Information includes four figures, five tables, Supplemental Experimental Procedures, and three movies and can be found with this article online at doi:10.1016/j.cub.2011.12.009.

Acknowledgments

We thank the assistance and advice of K. Eliceiri and J. White of the Laboratory for Optical and Computational Instrumentation supported by National Institutes of Health (NIH) grant RR00570. We also thank Y. Kohara (National Institute of Genetics, Mishima, Japan) for cDNAs, A. Fire (Stanford, CA) for GFP vectors, and N. Levy-Strumpf, T. Kawano, K. Fujisawa, and J. Plummer for their critical reading of the manuscript. Some worm strains were obtained from the Caenorhabditis Genetics Center, funded by the NIH National Center for Research Resources. This work was supported by an Ontario Graduate Scholarship to R.I. and by grants from the Canadian Institutes of Health Research (MOP 13207) and the NIH (NS41397) to J.C. K.S. and J.H. were supported by NIH grant GM058038 awarded to J.H.

Received: July 25, 2011
Revised: December 2, 2011
Accepted: December 5, 2011
Published online: December 22, 2011

References

1. Brewer, S., and Williams, T. (2004). Finally, a sense of closure? Animal models of human ventral body wall defects. Bioessays *26*, 1307–1321.
2. Fernández, B.G., Arias, A.M., and Jacinto, A. (2007). Dpp signalling orchestrates dorsal closure by regulating cell shape changes both in the amnioserosa and in the epidermis. Mech. Dev. *124*, 884–897.
3. Martin, P., and Parkhurst, S.M. (2004). Parallels between tissue repair and embryo morphogenesis. Development *131*, 3021–3034.
4. Orioli, D., Henkemeyer, M., Lemke, G., Klein, R., and Pawson, T. (1996). Sek4 and Nuk receptors cooperate in guidance of commissural axons and in palate formation. EMBO J. *15*, 6035–6049.
5. Compagni, A., Logan, M., Klein, R., and Adams, R.H. (2003). Control of skeletal patterning by ephrinB1-EphB interactions. Dev. Cell *5*, 217–230.
6. Roy, P.J., Zheng, H., Warren, C.E., and Culotti, J.G. (2000). mab-20 encodes Semaphorin-2a and is required to prevent ectopic cell contacts during epidermal morphogenesis in Caenorhabditis elegans. Development *127*, 755–767.
7. Nakao, F., Hudson, M.L., Suzuki, M., Peckler, Z., Kurokawa, R., Liu, Z., Gengyo-Ando, K., Nukazuka, A., Fujii, T., Suto, F., et al. (2007). The PLEXIN PLX-2 and the ephrin EFN-4 have distinct roles in MAB-20/Semaphorin 2A signaling in Caenorhabditis elegans morphogenesis. Genetics *176*, 1591–1607.
8. George, S.E., Simokat, K., Hardin, J., and Chisholm, A.D. (1998). The VAB-1 Eph receptor tyrosine kinase functions in neural and epithelial morphogenesis in C. elegans. Cell *92*, 633–643.
9. Chin-Sang, I.D., George, S.E., Ding, M., Moseley, S.L., Lynch, A.S., and Chisholm, A.D. (1999). The ephrin VAB-2/EFN-1 functions in neuronal signaling to regulate epidermal morphogenesis in C. elegans. Cell *99*, 781–790.
10. Chin-Sang, I.D., and Chisholm, A.D. (2000). Form of the worm: genetics of epidermal morphogenesis in C. elegans. Trends Genet. *16*, 544–551.
11. Wang, X., Roy, P.J., Holland, S.J., Zhang, L.W., Culotti, J.G., and Pawson, T. (1999). Multiple ephrins control cell organization in C. elegans using kinase-dependent and -independent functions of the VAB-1 Eph receptor. Mol. Cell *4*, 903–913.
12. Wang, X., Zhang, W., Cheever, T., Schwarz, V., Opperman, K., Hutter, H., Koepp, D., and Chen, L. (2008). The C. elegans L1CAM homologue LAD-2 functions as a coreceptor in MAB-20/Sema2 mediated axon guidance. J. Cell Biol. *180*, 233–246.
13. Priess, J.R., and Hirsh, D.I. (1986). Caenorhabditis elegans morphogenesis: the role of the cytoskeleton in elongation of the embryo. Dev. Biol. *117*, 156–173.
14. Henkemeyer, M., Orioli, D., Henderson, J.T., Saxton, T.M., Roder, J., Pawson, T., and Klein, R. (1996). Nuk controls pathfinding of commissural axons in the mammalian central nervous system. Cell *86*, 35–46.
15. Williams-Masson, E.M., Malik, A.N., and Hardin, J. (1997). An actin-mediated two-step mechanism is required for ventral enclosure of the C. elegans hypodermis. Development *124*, 2889–2901.
16. Ikegami, R., Zheng, H., Ong, S.H., and Culotti, J. (2004). Integration of semaphorin-2A/MAB-20, ephrin-4, and UNC-129 TGF-beta signaling pathways regulates sorting of distinct sensory rays in C. elegans. Dev. Cell *6*, 383–395.
17. Brenner, S. (1974). The genetics of Caenorhabditis elegans. Genetics *77*, 71–94.
18. Köppen, M., Simske, J.S., Sims, P.A., Firestein, B.L., Hall, D.H., Radice, A.D., Rongo, C., and Hardin, J.D. (2001). Cooperative regulation of AJM-1 controls junctional integrity in Caenorhabditis elegans epithelia. Nat. Cell Biol. *3*, 983–991.
19. Raich, W.B., Moran, A.N., Rothman, J.H., and Hardin, J. (1998). Cytokinesis and midzone microtubule organization in Caenorhabditis elegans require the kinesin-like protein ZEN-4. Mol. Biol. Cell *9*, 2037–2049.
20. Mohler, W.A., Simske, J.S., Williams-Masson, E.M., Hardin, J.D., and White, J.G. (1998). Dynamics and ultrastructure of developmental cell fusions in the Caenorhabditis elegans hypodermis. Curr. Biol. *8*, 1087–1090.
21. Sulston, J.E., Schierenberg, E., White, J.G., and Thomson, J.N. (1983). The embryonic cell lineage of the nematode Caenorhabditis elegans. Dev. Biol. *100*, 64–119.

Current Biology, Volume *22*

Supplemental Information

Semaphorin and Eph Receptor Signaling Guide a Series of Cell Movements for Ventral Enclosure in *C. elegans*

Richard Ikegami, Kristin Simokat, Hong Zheng, Louise Brown, Gian Garriga, Jeff Hardin, and Joseph Culotti

Supplemental Inventory

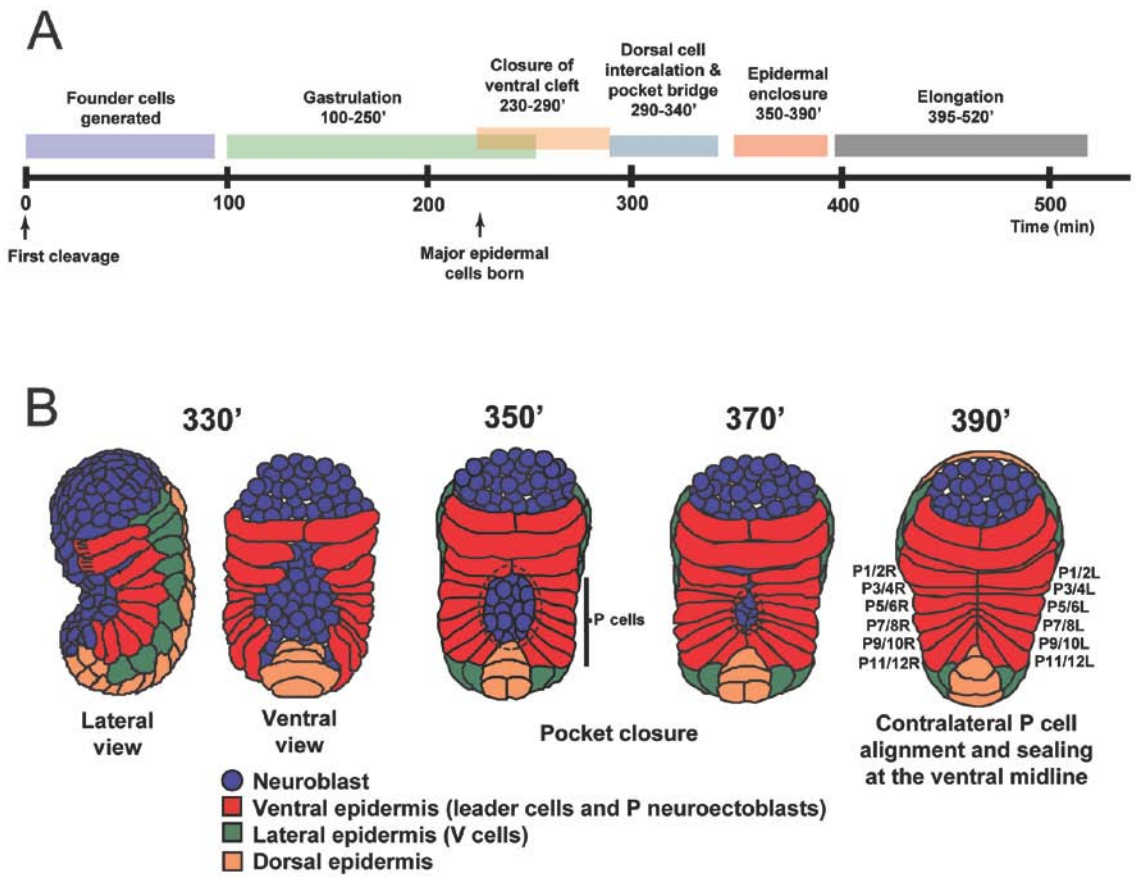

Figure S1. Pocket Closure in Wild-Type, *vab-1* Null and *mab-20* Null Mutant Embryos, Related to Figure 1

(A) Timing of developmental events at 20^{o}C after the first cell cleavage (PFC) of the embryo is indicated in minutes across the top.

(B) Schematic of the ventral enclosure process.

(C) All *Pplx-2::gfp* reporter expressing cells in the relevant region of the open pocket are shown. Only ventral plexin band cells are indicated by a colored font, corresponding to the colored squares used to represent these cells in Figures 1 and 2.

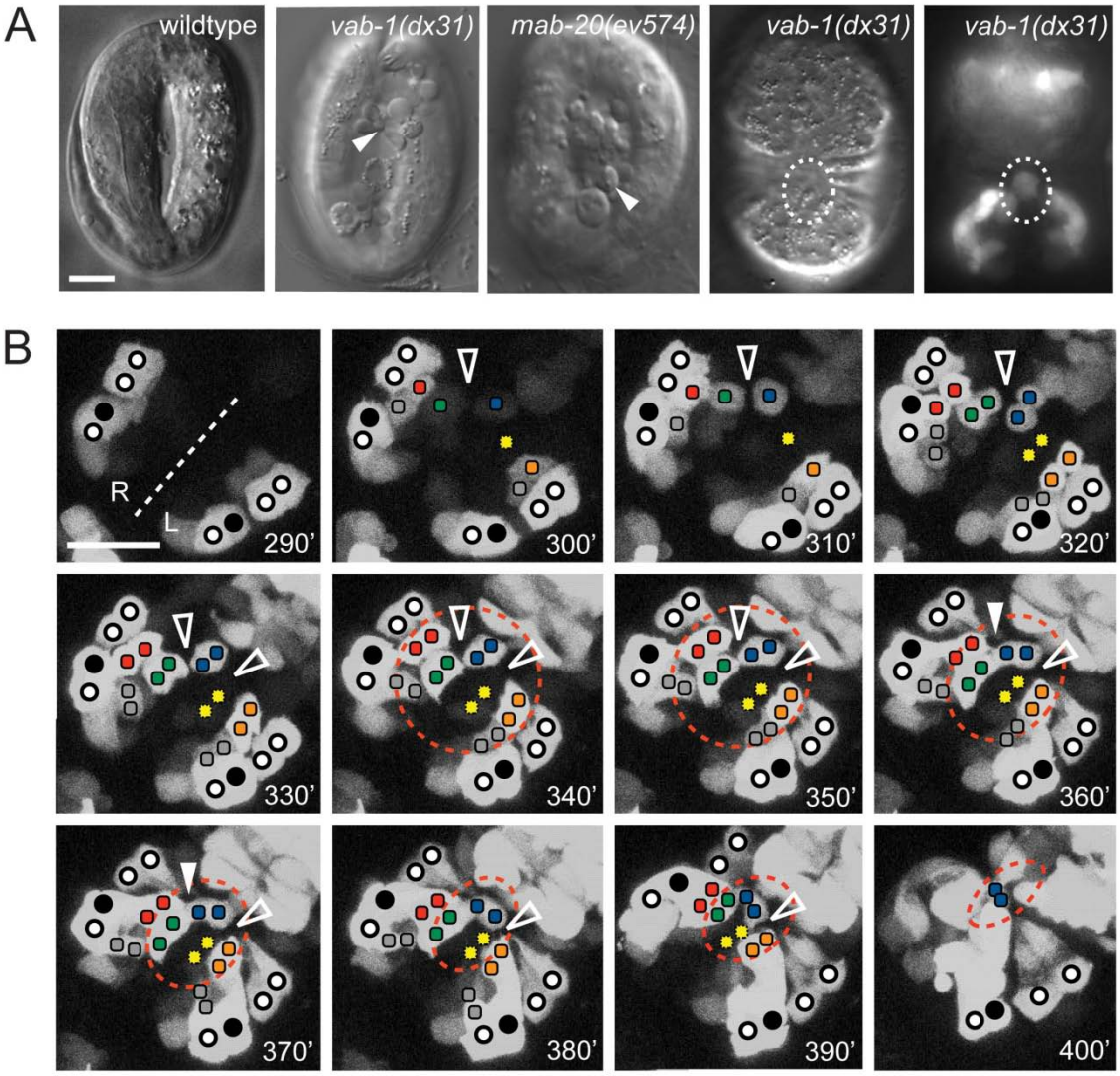
A
wildtype
vab-1(dx31)
mab-20(ev574)
vab-1(dx31)
vab-1(dx31)
B
R
L
290'
300'
310'
320'
330'
340'
350'
360'
370'
380'
390'
400'

Figure S2. *vab-1* Mutant Pocket Closure Phenotype, Related to Figure 2

(A) The first three frames left to right are DIC images of a wild type embryo (WT), a *vab-1(dx31)* null mutant embryo and a *mab-20(ev574)* null mutant embryo at the 3-fold stage of embryogenesis following ventral enclosure and elongation. The last two frames show a DIC and corresponding fluorescence (P*plx-2::gfp*) view of a *vab-1(dx31)* null comma stage embryo with a defective open pocket (circled).

(B) Time lapse of a *Pplx-2::gfp* reporter was used to follow pocket bridge formation and migration of the pocket cells in a *vab-1(dx31)* null mutant background. Ventral view of the pocket region. Anterior is to the top right. Dotted line represents the position of the midline separating right (R) and left (L) sides. Open and closed circles mark the P cells of the open pocket. The position of P9/10 during pocket closure is marked (closed black circle). Developmental time in minutes post-first cleavage (PFC) at 20^{o}C is shown at bottom right of each panel. Labeling of cell types is as in Figures 1 and 2. At 290-300' onset of *Pplx-2::gfp* reporter expression in the *vab-1* mutant begins and is identical to the wild type. At 310-320' there are gaps (310' open arrowhead) between scaffold cell precursors and between non-sister plexin band cells (320' open arrowhead) that are not observed in the wild type. These gaps persist until (330-350') on the right and perhaps later on the left. The red presumptive pocket bridge cell on the right appears to extend a short protrusion directly toward the blue cell on the right (360'). This protrusion is unlike the longer protrusions observed in wildtype embryos that extend over the intervening cells to the junction between the blue cells. At 360-390' the orange presumptive bridge cells on the left do not contact the blue central scaffold cell on the left even at 390' PFC due to the absence of protrusions from the orange to the blue cells normally observed in the wild type. At 400' the embryo begins to turn and elongate making it difficult to follow individual identified cells. An open pocket defect or hole of exposed neuroblasts is left on the ventral side of the embryo (dotted red circle). Constrictive forces of embryo elongation extrude internal cells through the open hole causing embryonic lethality. Scale bar, 10 μm.

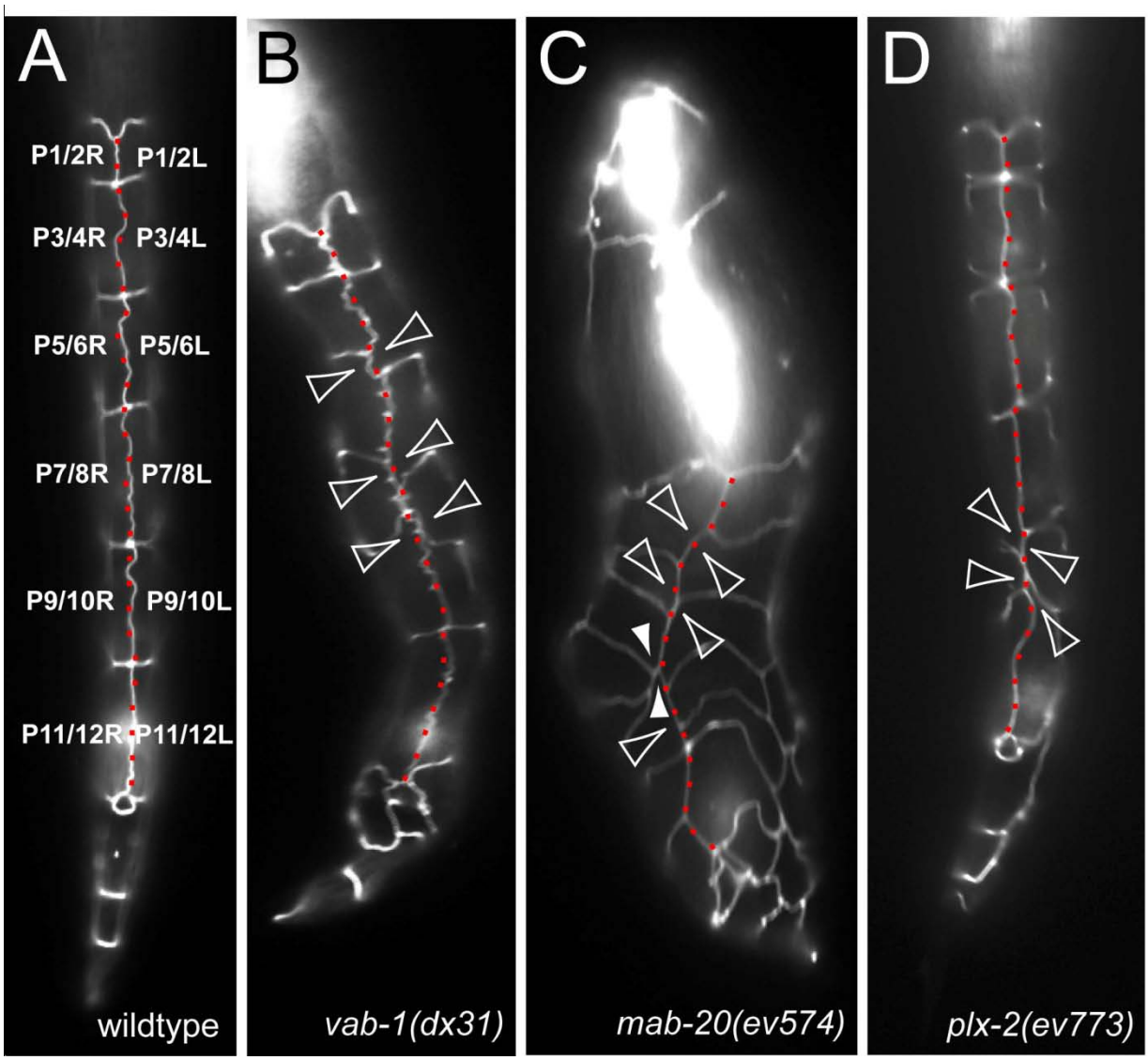
A
P1/2R
P1/2L
P3/4R
P3/4L
P5/6R
P5/6L
P7/8R
P7/8L
P9/10R
P9/10L
P11/12R
P11/12L
wildtype
B
vab-1(dx31)
C
mab-20(ev574)
D
plx-2(ev773)

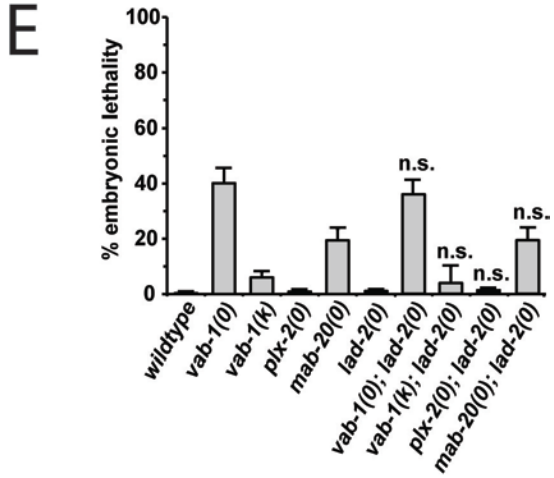
E
% embryonic lethality
100
80
60
40
20
0
n.s.
n.s.
n.s.
n.s.
wildtype
vab-1(0)
vab-1(k)
plx-2(0)
mab-20(0)
lad-2(0)
vab-1(0); lad-2(0)
vab-1(k); lad-2(0)
plx-2(0); lad-2(0)
mab-20(0); lad-2(0)

Figure S3. P Cell Alignment at the Ventral Midline in Wild-Type and Mutant L1 Larvae and *lad-2* Mutant Embryonic Lethality, Related to Figure 5

Anterior is up. Ventral view of L1 larvae expressing AJM-1::GFP, an adherens junction marker outlining P cell boundaries and showing the ventral midline (dotted red line).

(A) wildtype larvae show precise contralateral P cell alignment at the midline.

(B-D) *vab-1*, *mab-20* and *plx-2* mutations cause abnormal adhesions between contralateral P cells (open arrowheads), whereas, *mab-20* mutations also cause abnormal ipsilateral adhesions (closed arrowheads).

(F) The percentsage of lethal embryos for various mutants including mutants of *lad-2*, which encodes a MAB-20/semaphoring-2A receptor, are shown. Error bars represent the standard deviation of a binomial distribution of the same sample size and observed mean.

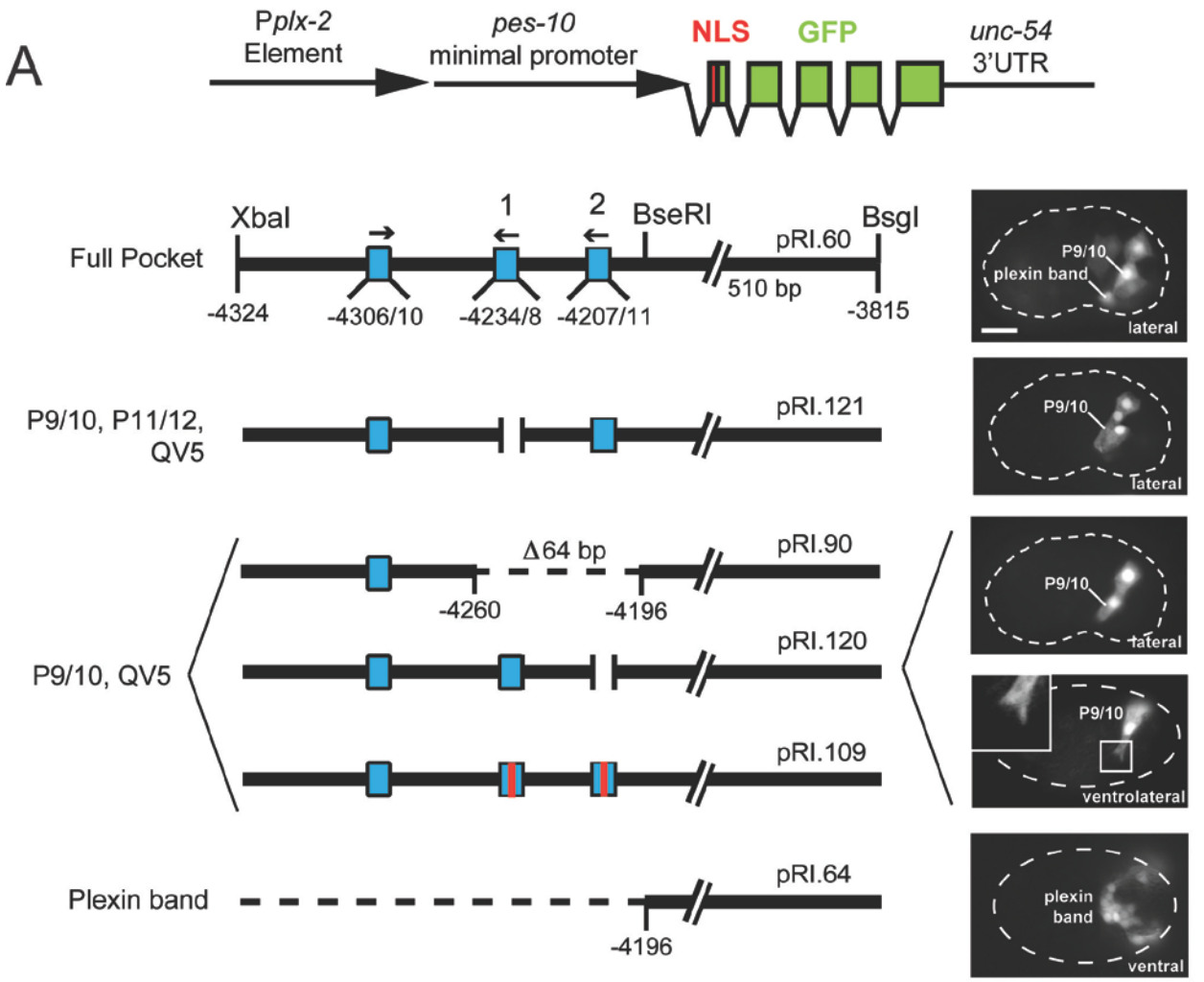
A
Pplx-2 Element
pes-10 minimal promoter
NLS
GFP
unc-54 3'UTR
Full Pocket
XbaI
1
2
BseRI
BsgI
pRI.60
510 bp
-4324
-4306/10
-4234/8
-4207/11
-3815
P9/10
plexin band
lateral
P9/10, P11/12, QV5
pRI.121
P9/10
lateral
P9/10, QV5
Δ64 bp
pRI.90
-4260
-4196
pRI.120
pRI.109
P9/10
lateral
P9/10
ventrolateral
Plexin band
pRI.64
-4196
plexin band
ventral
B
Eph
FNIII
FNIII
TM
Tyr Kinase
SAM
PDZ binding
1
100
200 aa
Region deleted in VAB-1(delC)
C
P9/10 or plexin band element
pes-10 minimal promoter
TM
vab-1 3' UTR
D
P9/10 or plexin band element
pes-10 minimal promoter
TM
GFP
unc-54 3' UTR

Figure S4. Identification of P9/10 and Plexin Band Cell-Specific Promoter Elements in the *plx-2* Promoter and Their Use in Driving Expression of *vab-1(+)* and *vab-1(delC)* for Transgenic Rescue Experiments, Related to Figure 6

(A) Various fragments of the *plx-2* promoter region were cloned 5' of the *pes-10::gfp* minimal promoter, pPD97.78 (Fire vector kit) which is commonly used to identify and characterize the cell specificity of action of promoter regulatory elements [1]. A 510 bp regulatory region of the *plx-2* promoter (Full Pocket element) drives spatio-temporal expression within the cells of the pocket (as in Figure S1C and shown to the right, inset showing expanded leading edge of P9/10 as in Figure 4H). Sequence alterations in this regulatory element that further restricted expression to P9/10 and Q5 or the plexin band (indicated to the left of the relevant constructs) included: (1) pRI.90, a deletions indicated by a dashed line, (2) pRI.120, deletions of homeobox core sequence TAAN (blue box) indicated by a gap in the sequence, and (3) pRI.109, point mutations (TAAA to TACG) indicated by a red bar within the homeodomain blue box, and (4) pRI.64, a deletion of the entire element. Expression patterns for these constructs are shown to the right. We then used the promoter elements identified by pRI.64 and pRI.90 to drive expression of *vab-1* transgenes in plexin band and P9/10 cells, respectively.

(B) Domain structure of VAB-1 and VAB-1(delC) are shown (Eph, FNIII, and TM are abbreviations for ephrin, fibronectin type III, and trasmembrane domains.

(C-D) 5’ regulatory regions of *plx-2* shown in panel A (pRI.64 and pRI.90) were used in conjunction with the *pes-10* promoter to drive expression of the *vab-1(+)* (C) and *vab-1(delC)* (D) gene constructs in the plexin band (pRI.64) or in P9/10 (pRI.90) as reported in Table S5. The 3’ UTRs were from the *vab-1* gene (panel A) or from *unc-54* (panel B).

Table S1. Summary of *plx-2* and *vab-1* Reporter Constructs and Transgene Arrays Made with These Constructs, Related to Figure 1

Transgene array	**Use of array**	**Name, structure and derivation of plasmid used in array[(1)]**	**5'UTR regulatory sequence[(2)]**	**Co-transformation gene[(3)] & co-injection method**	**Name of strain carrying array[(4)]**
evIs190 II	Transcriptional Reporter	*pRI.70* *Pvab-1::venus* (*Pvab-1* cloned into *pPD95.79*_venus)	2369 bp promoter	*pRF4*(50 ng/µl) + *pRI.70*(50 ng/µl)	NW1692
evIs168 V	translational reporter	*pZH155* *Pplx-2::PLX-2::GFP + plx-2 3'UTR (genomic ApaI-EcoRI fragment cloned into pBluescript SKII+ then spliced to GFP)*	4900 bp promoter	*pRF4*(50 ng/µl) + *pZH155*(50 ng/µl)	NW1635
evIs136 V	transcriptional reporter	*pRI.20* *Pplx-2::gfp* (*Pplx-2* cloned into *pPD95.75*)	4529 bp promoter	*pRF4*(50 ng/µl) + *pRI.20*(50 ng/µl)	NW1545
evIs191	transcriptional reporter	*pRI.21* *Pplx-2::cfp* (*Pplx-2* cloned into *pPD122.66*)	4529 bp promoter	*pRF4*(50 ng/µl) + *pRI.21*(50 ng/µl)	NW1693

(1) *pPD97.78* were provided by Dr. A. Fire. Details are available at www.addgene.org/Andrew_Fire.

(2) 5' regulatory regions comprise the number of base pairs (bp) shown located upstream of the initiator methionine codon for each gene.

(3) *pRF4* carries the dominant roller gene *rol-6(su1006.)*

(4) Strain names are indicated on the same line as the transgene array they carry as indicated in the first column.

Table S2. Penetrance (% of Animals) of Four Pocket Closure Defects Observed in Various Mutants, Related to Figure 5

Genotype	% Obstructed Bridge	n	% sister cell gaps	n	% P cell misalignment	n	% embryonic lethality (±SEM)	n
Wild type	2	136	0	136	1	147	0.27 ± 0.32	1464
vab-1(0)	97	134	1	134	12	162	40.1 ± 5.48	1818
vab-1(k)	91	121	0	121	3	161	5.97 ± 2.12	2980
plx-2(0)	2	142	0	142	8	173	0.83 ± 0.71	2284
mab-20(0)	5	130	0	130	86	137	19.4 ± 4.11	2175
mab-20(0); plx-2(0)	4	123	1	123	88	137	23.38 ± 7.8	1300
vab-1(0) plx-2(0)	96	136	48*	136	34*	168	74.82* ± 6.37	2761
vab-1(k) plx-2(0)	95	127	2	127	13	142	8 ± 5.49	3133
mab-20(0); vab-1(0)†	100	53	100*	53	ND	-	100*	78
mab-20(0); vab-1(k)†	100	45	100*	45	100¶*	38	98*	115

† *mab-20(0); vab-1(0)* and *mab-20(0); vab-1(k = kinase dead)* double mutants are derived from *mIn1mIs14* balanced lines [2] *mab-20(0); vab-1(k)/mIn1mIs14*; and *mab-20(0); vab-1(0)/mIn1mIs14*. *mIs14* carries an expressing GFP gene, so homozygous double null segregants are non-GFP.ND = not determined. Since our assay for cell alignment defects use L1 escapers, we are unable assess these defects in the *mab-20(0); vab-1(0)* animals precluded by the fully penetrant embryonic lethality. ¶ P cell alignment defects in the *mab-20(0); vab-1(k)* background were determined for rare L1 escapers among non-GFP segregants of *mab-20(0); vab-1(k)/mIn1mIs14*. Two-sided Fisher's Exact Test was used as the statistical test for genetic interaction of; obstructed bridge defects, sister plexin band cell gaps, and P cell misalignment defects. A two-sided t-test was used as the statistical test for genetic interaction of embryonic lethality except for interactions involving *mab-20(0); vab-1(0)* and *mab-20(0); vab-1(k)* for which a two-sided Fisher's Exact Test was used, $P = 0.05$ was used as the cutoff for significance, * $P < 0.0001$ (see Experimental Procedures).

Table S3. Cell-Type Specific Rescue Experiments[1], Related to Figure 6

Transgene	Genotype	% Obstructed bridge [2]	n	Rescue	% P cell misalignment[2]	n	Rescue	% embryonic lethality[3]	n	Rescue
	vab-1(0)	97	134		12	168		40.1 ± 5.5	1818	
	vab-1(0) plx-2(0)	96 (48)	136		34	162		74.8 ± 6.4	2761	
P_plexin band:: *vab-1(+)*	*vab-1(0); evls261*	4	115	+*	2	242	+*	1.5 ± 1.4	1039	+*
	vab1(0); evls262	4	139	+*	4	143	+¶	1.8 ± 1.3	2786	+*
	vab1(0); evls263	43	129	+*	10	168	-	ND		
	vab1(0); evls264	14	133	+*	6	249	+¶	ND		
	vab-1(0) plx-2(0); evls261	17 (4)	153	+* (+*)	11	181	+†	2.7 ± 1.7	1824	+*
P_plexin band:: *vab-1(delC)*	*vab-1(0); evls329*	97	131	-	31	203	+*	0.7 ± 0.6	1536	+*
	vab1(0); evls330	95	141	-	6	163	-	1.8 ± 1.4	1409	+*
	vab1(0); evls331	94	133	-	4	139	+¶	1.8 ± 1.1	2092	+*
	vab1(0); evls332	98	123	-	ND			ND		
	vab1(0) plx-2(0); evls331	93 (6)	133	- (+*)	13	262	+*	3.1 ± 4.1	2150	+*
P_P9/10:: *vab-1(+)*	*vab1(0); evls236*	72	129	-	14	147	-	3.2 ± 1.5	1978	+*
	vab1(0); evls237	66	105	-	11	175	-	3.9 ± 1.6	2374	+*
	vab1(0); evls238	97	139	-	13	153	-	1.8 ± 1.4	1630	+*
	vab1(0); evls239	96	142	-	14	158	-	2.5 ± 1.6	2032	+*
	vab1(0) plx-2(0); evls238	93 (52)	165	- (-)	26	222	-	42.2 ± 8.8	1205	+*
P_P9/10:: *vab-1(delC)*	*vab1(0); evls325*	98	132	-	19	108	-	51.4 ± 6.8	1877	-
	vab1(0); evls326	99	115	-	24	234	-	58.6 ± 8.9	2020	-
	vab1(0); evls327	94	207	-	17	158	-	38.4 ± 6.1	3931	-
	vab-1(0); evls328	96	125	-	17	134	-	33.4 ± 7.7	2636	-
	vab1(0) plx-2(0); evls327	95 (47)	170	- (-)	25	214	-	37.8 ± 3.7	1061	+*

(1) Data from shaded rows are presented in Figure 6. + = rescue. - = no rescue. ND = not determined. Values in parentheses in the "% obstructed bridge column" represent % of plexin bands showing sister cell gaps with corresponding rescue result ('+' or '-') also in parentheses. **(2)** Two-sided Fisher's Exact Test was used as the statistical test for rescue of obstructed bridge defects, and P cell misalignment defects. **(3)** Two-sided t-test was used as the statistical test for rescue of embryonic lethality. To determine the significance of rescue, P = 0.05 was used as the cutoff for significance, * $P < 0.0001$, † $P < 0.001$ and ¶ $P < 0.05$ (see Experimental Procedures).

Table S4. Summary of Reporter Constructs to Identify Cell-Type Specific Promoter Elements from the *plx-2* 5' Regulatory (i.e., Promoter) Region, Related to Figure 6

Transgene array	**Name, structure and derivation of plasmid used in array[(1)]**	**5'UTR regulatory sequence[(3)]**	**Co-transformation gene[(4)] & co-injection method**	**Name of strain carrying array[(5)]**
evIs194 full pocket promoter	*pRI.60* *XbaI-BsgI* fragment of *Pplx-2* cloned upstream of *pes-10* promoter in *pPD97.78 (NLS::GFP)*	510 bp	*pRF4*(50 ng/µl) + *pRI.60*(50ng/µl)	NW1707
evIs195 P9/10 (QV5) - specific promoter	*pRI.90* = *pRI.60* with 64 bp internal deletion (-4260 to -4196)	446 bp	*pRF4*(50 ng/µl) + *pRI.90*(50 ng/µl)	NW1708
evEx394 plexin band-specific promoter	*pRI.64* = *pRI.60* deleted *XbaI* to *BseRI*	380 bp	*pRF4*(50 ng/µl) + *pRI.64*(50 ng/µl)	NW2085
evIs201 *evIs202* *evIs204* *evIs208*	*pRI.109* = *pRI.60* mutated for both TAAA sites in *plx-2* promoter to TACG[(2)]	mutant of TAAA to TACG #1 and #2	*pRF4*(50 ng/µl) + *pRI.109*(50 ng/µl)	NW1714 NW1718 NW 1720 NW1728

(1) *pPD97.78* were provided by Dr. A. Fire. Details are available at www.addgene.org/Andrew_Fire.

(2) See red bars in Figure S4.

(3) Size (bp) of the 5' regulatory regions of the *plx-2* promoter used to clone upstream of the *pes-10* minimal promoter.

(4) *pRF4* carries the dominant roller gene *rol-6(su1006).*

(5) Strain names are indicated on the same line as the transgene array they carry as indicated in the first column. High-copy integrations were done by UV (see Supplemental Experimental Procedures). High copy number integrations of arrays into the genome were by UV irradiation (see Supplemental Experimental Procedures).

Table S5. Summary of Constructs Used to Drive Expression of *vab-1(+)* or *vab-1(delC)* in P9/10 Cells or in Plexin Band Cells, Related to Figure 6

Transgene array	**Use of array**	**Name, structure and derivation of plasmid used in array[(1)]**	**5'UTR regulatory sequence[(2)]**	**Co-transformation gene[(3)] & co-injection method**	**Name of strain carrying array[(4)]**
evIs261 *evIs262* *evIs263* *evIs264*	Plexin band-specific rescue with *vab-1(+)*	*pZH209* *= P_plexin band::VAB-1(+) + vab-1 3'UTR* promoter from *pRI.64* (see above) upstream of *pes-10* promoter	see Fig S5 (and below)	*unc-119(+) + pZH209* into *unc-119(e2498)*	NW1791 NW1792 NW1793 NW1794
evIs329 *evIs330* *evIs331* *evIs332*	Plexin band-specific rescue with *vab-1(delC)*	*pZH217* *= P_plexin band::VAB-1(delC)::GFP + unc-54 3'UTR* promoter from *pRI.64* (see above) upstream of *pes-10* promoter	see Fig S5 (and below)	*unc-119(+) + pZH217* into *unc-119(e2498)*	NW1858 NW1859 NW1860 NW1861
evIs236 *evIs238* *evIs239* *evIs240*	P9/10-specific rescue with *vab-1(+)*	*pZH198* *= P_P9/10::VAB-1(+) + vab-1 3'UTR* promoter from *pRI.90* (see above) upstream of *pes-10* promoter	see Fig S5 (and below)	*unc-119(+) + pZH198* into *unc-119(e2498)*	NW1765 NW1766 NW1767 Nw1768
evIs325 *evIs326* *evIs327* *evIs328*	P9/10-specific rescue with *vab-1(delC)*	*pZH216* *= P_P9/10::VAB-1(delC)::GFP + unc-54 3'UTR* promoter from *pRI.90* (see above) upstream of *pes-10* promoter	see Fig S5 (and below)	*unc-119(+) + pZH216* into *unc-119(e2498)*	NW1854 NW1855 NW1856 NW1857

(1) *pRI.64* and *pRI.90* are plexin band-specific and *P9/10*-specific promoters, respectively, whose derivation is indicated in Figure S4.

(2) 5' regulatory regions of the *plx-2* promoter are as described in previous column and depicted in Figure S5.

(3) Co-transformation and integration was determined by rescue of the *unc-119(e2498)* mutant uncoordinated phenotype. Bombardment was used to establish low-copy integration of these transgenes (see Supplemental Procedures).

(4) Strain names are indicated on the same line as the transgene array they carry as indicated in the first column.

Supplemental Experimental Procedures

Cell-Type-Specific Rescue of the *mab-20; vab-1* Double-Mutant Ventral Enclosure Phenotypes

In *mab-20(0); vab-1(0)* or *mab-20(0); vab-1(e2)* (kinase-dead) double mutants, the pocket bridge cells are found in the correct numbers, but are rounded and highly separated from one another. These severe defects cause 100% lethality for the double null and roughly 98% embryonic lethality for the *mab-20; vab-1(e2)* double mutant. All of the double null mutant embryos die with an open pocket. Roughly 2% of *mab-20; vab-1(e2)* survivors die as larvae with highly misaligned P cells and severe body morphology defects.

We determined semi-quantitatively the ability of *vab-1(+)* and *vab-1(delC)* expressed in the plexin band and P9/10 to rescue the embryonic lethality of the *mab-20; vab-1* double null. All combinations except *vab-1(delC)* expressed in P9/10 rescued about 30% of embryos from embryonic lethality with about two-thirds of these dying as L1 larvae, whereas *vab-1(delC)* expressed in P9/10 showed no rescue. Roughly two-thirds and one-third of the rescued embryos from the three partially rescuing lines died as L1 or L2 larvae, respectively; however, rare animals survived to adulthood and produced very small broods and were difficult to propagate. The high embryonic lethality observed in these cell-type specific rescue experiments suggests the existence of a greater synergy between MAB-20 and VAB-1 than between PLX-2 and VAB-1 function for closure of gaps between sister plexin band cells, consistent with our demonstration that MAB-20 has PLX-2-dependent and -independent functions (Figure 5D), however, the cell-specificity of phenotypic rescue is basically the same as for the *vab-1 plx-2* double null, and is consistent with the pattern of redundancies diagrammed in Figure 5D.

Calculation of Expected Lethality Based on Absence of Effect of the *plx-2* Null Mutation on Migration over an Obstructed Pocket Bridge

An important question arising from these results is whether the *plx-2* mutation in the *vab-1 plx-2* double null embryos hinders P cell migration on an obstructed bridge more than in the *vab-1* null mutation alone. Evidence against this idea is provided by the measured frequency of double mutant lethality compared to that predicted if the *plx-2* mutation has no effect on migration over an obstructed bridge. Embryonic lethality based on the penetrance of sister plexin band cell gaps is 48% (Figure 5), which suggests that 40% of the remaining 52% (or 21%) are predicted to die because of a *vab-1* mutant deficit in P9/10 migration over an obstructed bridge. This predicts a penetrance of 48% plus 21% or 69% embryonic lethality in the double, which is not significantly different from what is observed (75%, Figure 5C, Table S2). Thus in the double mutant, a *plx-2* deficit does not further hinder P9/10 progression over an obstructed bridge to the ventral midline, rather hindrance of P cell migration over an obstructed bridge, results from the *vab-1* deficit alone, whereas obstruction by sister cell gaps results only from a deficit in both *vab-1* and *plx-2*.

Transgene Rescue of Double Mutants

Since *mab-20(0); vab-1(0)* and *mab-20(0); vab-1(e2)* are completely embryonic lethal we used balancer *mIn1mIs14* [2] to balance the *vab-1* locus on LG II in *mab-20(0); vab-1(dx31)* and *mab-20(0); vab-1(e2)* double mutants. *mIn1mIs14* is an inversion of LGII. This inversion carries *myo-2::gfp*; gut *enhancer::gfp* and a *dpy-10(e128)* mutation. We constructed lines containing: (a) *mab-20(0); vab-1(0)/mIn1mIs14; evIs261[P_plexin band::vab-1(+); unc-119(+)]* and (b) *mab-20(0); vab-1(0)/mIn1mIs14; evIs331[P_plexin band::vab-1(delC); unc-119(+)]* and (c) *mab-*

20(0); vab-1(0)/mIn1mIs14; evIs238[P_P9/10::vab-1(+); unc-119(+)] and (d) *mab-20(0); vab-1(0)/mIn1mIs14; evIs325[P_P9/10::vab-1(delC); unc-119(+)]* and analyzed non-fluorescing progeny that lack the balancer and should be homozygous for *vab-1(dx31)*.

Reporter and Rescue Constructs

Reporter and cell type specific rescue constructs are summarized in Tables S3-S5.

***vab-1(+)* Construct**

vab-1(+), which includes the *+ vab-1 3'UTR*, was cloned downstream of the *pes-10* minimal promoter (*pes-10* was derived from *pPD97_78* - see www.addgene.org/Andrew_Fire) replacing the *NLS*, *GFP* and the *unc-54 3'UTR*. Cell-specific promoter elements were cloned upstream of *pes-10*. An unspliced minigene comprises the first 4 introns, the first 4 exons plus part of exon 5 of *vab-1* (+). The remaining coding sequence is from a *vab-1* cDNA that was cloned downstream of exon 5. This construct contains 763 bp of the *vab-1 3' UTR* downstream of the stop codon.

***vab-1(delC)* Construct Encodes a C-Terminal Truncated Version of VAB-1(+) Fused to GFP + *unc-54* 3' UTR**

vab-1(delC) was cloned downstream of the *pes-10* minimal promoter (*pes-10* was derived from *pPD97_78*). A unique *BamHI* site downstream of the TM domain of the *vab-1* cDNA was used to clone *GFP* as an in-frame fusion with the *unc-54* 3' UTR. This generates a C-terminal deletion product containing an 89 a.a. intracellular sequence downstream of the transmembrane (TM) domain (ie. 267 bp of *vab-1* cDNA sequence downstream from the TM domain at the *BamHI* site) fused to GFP.

Transformation and Transgene Integration Procedures

Ballistic transformation was as described in [3]. Except for *jcIs1*[*AJM-1::GFP*] and for reporter lines, L4 hermaphrodites carrying extrachromosomal arrays of the transgene of interest were stably integrated by ultraviolet irradiation at 300 μJ x 100 in a Stratalinker (Stratagene) and backcrossed to N2 at least three times.

***plx-2(ev773)* PCR Genotyping**

A multiplex PCR-based genotyping assay was used to confirm the presence and zygosity of the *plx-2(ev773)* allele. Primer PLX.1F (5'-ACTCATTTCCCCTCATTTTACG-3') directed to 5' sequence outside of the deletion and primer PLX.27F (5'-TCGCGGGAACAACAACTTCGC-3'), directed to sequence within the deleted region was mixed with common PLX.14R (5'-ACCATTTTGCTGACCTCGC-3') primer. A wildtype allele generates a 334 bp product, whereas a deletion allele generates a 249 bp product.

Supplemental References

1. Teng, Y., Girard, L., Ferreira, H.B., Sternberg, P.W., and Emmons, S.W. (2004). Dissection of cis-regulatory elements in the C. elegans Hox gene egl-5 promoter. Dev Biol *276*, 476-492.
2. Edgley, M.L., and Riddle, D.L. (2001). LG II balancer chromosomes in Caenorhabditis elegans: mT1(II;III) and the mIn1 set of dominantly and recessively marked inversions. Mol Genet Genomics *266*, 385-395.
3. Wilm, T., Demel, P., Koop, H.U., Schnabel, H., and Schnabel, R. (1999). Ballistic transformation of Caenorhabditis elegans. Gene *229*, 31-35.